TAMPERE UNIVERSITY OF TECHNOLOGY
Degree Programme in
Science and Engineering

Jari Tapani Kolehmainen

Simulation of assist gas flow in laser cutting with high performance nozzles.

Master of Science Thesis

Subject approved by the Department Council on 6.2.2013
Examiners: Prof. Robert Piché (TUT),
D.Sc(Tech) Simo Ali-Löytty (TUT)

ABSTRACT

TAMPERE UNIVERSITY OF TECHNOLOGY
Master's Degree Programme in Science and Engineering
KOLEHMAINEN, JARI TAPANI: Simulation of assist gas flow in laser cutting with high performance nozzles.
Master of Science Thesis, 81 pages, 2 Appendix pages
Autumn 2011
Major: Mathematics
Examiners: Prof. Robert Piché and D.Sc Simo Ali-Löytty
Keywords: Laser cutting, Laval nozzle, CFD

This thesis aims to present a computational fluid dynamics (CFD) model of the assist gas flow in laser cutting. This model is intended to aid in the design of nozzles. A brief discussion of laser cutting processes is also included in order to understand the role of an assist gas in the laser cutting process.

Simulation was done using the CFD software Star-CCM+. Simulations were executed using a segregated solver instead of a coupled one in order to keep the simulations computationally inexpensive. This is particularly important when the model becomes more complex by introduction of chemical reactions or molten metal particles. Two different viscosity models were used, namely the Sutherland law and a constant viscosity model. Results obtained by these two models were similar. However the use of the Sutherland law resulted in numerical problems. Thus, it can be concluded that the constant viscosity model is more suitable in this study case.

Comparison with the Schlieren photographs show that the developed CFD model is adequate to predict flow of a Laval nozzle.

Tiivistelmä

TAMPEREEN TEKNILLINEN YLIOPISTO
Teknis-luonnontieteellinen koulutusohjelma
KOLEHMAINEN, JARI TAPANI: Apukaasuvirtauksen simulointi laser leikkauksessa.
Diplomityö, 81 sivuja, 2 liitesivua
Elokuu 2011
Pääaine: Matematiikka
Tarkastajat: Prof. Robert Piché ja TkT. Simo-Ali-Löytty
Avainsanat: Laser leikkaus, Laval suutin, CFD

Työn päämääränä oli esittää laskennallinen CFD-malli apukaasuvirtaukselle laser leikkauksessa. Mallin tarkoituksena on auttaa apukaasusuutinten suunnittelussa. Työssä käsiteltiin myös apukaasun roolia laser leikkauksessa, jotta lukija kykenisi paremmin ymmärtämään työn päämäärää.

Simulaatiot suoritettiin Star-CCM+ CFD-ohjelmistolla. Simuloinnissa käytettiin tavanomaista eriytettyä ratkaisijaa yhdistetyn ratkaisijan sijasta, jotta laskenta voitaisiin pitää mahdollisimman kevyenä. Tästä on erityisesti hyötyä, kun monimutkaisempia malleja yhdistetään kaasuvirtaukseen. Työssä vertailtiin myös kahta eri viskositeetti mallia. Malleiksi valittiin Sutherlandin-laki ja vakio viskositeetti malli. Molemmat mallit antoivat samankaltaisia tuloksia, mutta Sutherlandin-lain käyttö aiheutti numeerisia ongelmia. Tästä syystä vakio viskositeetti malli oli sopivampi kyseiseen ongelmaan.

Laskentatulosten paikkansapitävyyttä arvioitiin Schelieren-kuvien avulla. Vertailussa tultiin lopputulokseen, että kyseinen malli pystyi ennustamaan kaasuvirtauksen Laval-suuttimessa riittävän hyvin.

Preface

This thesis was made during summer and fall of 2011, while I was an exchange student at the University of Okayama in Japan. I would like to thank Assistant Professor Yasuhiro Okamoto, Doctor Simo Ali-Löytty and Professor Robert Piché for help and advice that I have received during the process. In addition I would like to thank B.Sc Hibiki Yamamoto for his help in the simulation and measurements of assist gas flow and Timo Viitanen for his help in the grammar.

Okayama, 19th September 2011

Jari Tapani Kolehmainen

Contents

Symbols

$\emptyset$	Empty set
$\mathbb{R}$	Set of real numbers
$\mathbb{R}^n$	n-dimensional real vector space
$\mathbb{N}$	Set of natural numbers $0, 1, 2, \ldots$
$\mathbb{N}^n$	n-dimensional natural number space i.e. multi-indexes
$\Omega \subset \mathbb{R}$	Ω is a subset of $\mathbb{R}$
$\partial\Omega$	Boundary of domain Ω
$C(\Omega)$	Set of continuous functions in Ω
$C_0(\Omega)$	Set of functions that have compact support
$C^n(\Omega)$	Set of functions that have continuous derivatives of order n
$W^{k,p}(\Omega)$	Sobolov space
$\sup f$	Supremum of function f
$\inf f$	Infimum of function f
ess sup f	Essential supremum of function f
$\langle \cdot, \cdot \rangle$	Inner product
$\|\cdot\|$	Norm
$\mathscr{L}$	Differential operator
∇	Gradient
$\nabla\cdot$	Divergence
∇^2	Laplace operator
$\nabla\times$	Curl
Du/Dt	Substantial derivative
δ_{ij}	Kronecker delta function
$\delta(\cdot)$	Dirac's delta function
$H(\cdot)$	Heaviside function
$\mathbf{f}$	Vector or tensor
$\mathbf{\Phi}$	Flux tensor
λ	Wavelength
f	Wave frequency
η	Efficiency
$\mathbf{E}$	Electric field

$\mathbf{B}$	Magnetic field
$\mathbf{\Pi}$	Stress tensor
$\mathbb{T}$	Viscous stress tensor
$\mathbf{u}$	Flow velocity
M	Mach number, molar mass
V	Volume
ν	Specific volume
p	Pressure, momentum
p_S	Stagnation pressure
T	Temperature
T_S	Stagnation temperature
ρ	Density
s, S	Entropy
h, H	Enthalpy
e, E	Energy
u, U	Internal energy
Q	Heat
W	Work
$\mathbf{q}$	Heat flux
Ψ	Dissipation function
$\overline{u}$	Time average of function u
$k^{'}$	Turbulent kinetic energy
$\varepsilon^{'}$	Turbulent dissipation rate
μ	Viscosity, first viscosity
$\mu^{'}$	Second viscosity
κ	Bulk viscosity
μ_T	Turbulent viscosity
μ_M	Mach angle
μ_0	Permeability in vacuum
ϵ_0	Permittivity in vacuum
h	Planck's constant
B_{21}, B_{12}	Einstein B constant
R	Ideal gas constant
R_M	Ideal gas constant divided by molar mass
C_S	Sutherland's constant
c_V	Heat capacity in constant volume
c_p	Heat capacity in constant pressure
c	Speed of wave; speed of light or sound
N_F	Fresnel number
γ	Adiabatic constant equal to 1.4 for air
β	Coefficient of thermal expansion

Pr_T	Prandtl number
Re	Reynolds number
$C_{\varepsilon i}$	Coefficients of k-ε model
$O(\cdot)$	O-function
C_ν	Courant number
Δx	Cell length
Δt	Time step

Abbreviations

DO	Differential Operator
SGDO	Semi Generalized Differential Operators
GDO	Generalized Differential Operators
PDE	Partial Differential Equation
FVM	Finite Volume Method
SFL	Slow Flow Laser
FAFL	Fast Axial Flow Laser
FTFL	Fast Transverse Flow Laser
HAZ	Heat Affected Zone
LASOX	Laser Assisted Oxygen Cutting
RANS	Reynolds Averaged Navier-Stokes
SIMPLE	Semi-Implicit Method for Pressure-Linked Equations
PISO	Pressure Implicit with Splitting of Operators
AMG	Algebraic Multigrid Method

Chapter 1

Introduction

As a cutting method, laser cutting has been becoming more popular. This is due to its advantages over other cutting methods such as plasma cutting or mechanical cutting methods. Laser cutting usually has good cut characteristics, it is fast and involves only very small wear in parts.

On the other hand, lasers may consume high amounts of electrical power. For instance a 100kW carbon dioxide laser may use up to 1MW electrical power. Apart from electricity the only major running cost is assist gas consumption. In particular the cut characteristics are improved if more assist gas, which is used to remove material from the cut is used. However this increases the running costs due to the increased consumption of the assist gas, which is typically nitrogen or oxygen. Hence, there is need for nozzle design that improves cut characteristics while consuming less assist gas.

Nozzles in laser cutting have typically been straight nozzles. Advantages of straight nozzles are simplicity and low initial cost. However, these nozzles do not accelerate assist gas and are far from optimal for purposes of cutting most materials. In this thesis we consider the so called Laval nozzle design, which enables to accelerate assist gas velocity to the supersonic domain.The high velocity provided by a supersonic jet is a highly desirable property in thin metal plate cutting, which is a typical application of laser cutting.

Nozzles can be designed by the so called ”trial and error” approach using laboratory tests with physical prototypes, which gives first hand knowledge of subject, but is slow and expensive. This is due to manufacturing difficulties involved in laser nozzle construction. The diameter of a nozzle may be as small as 0.1 mm, hence making precision machining slow and expensive.

The more intelligent approach of using computational fluid dynamics (CFD) models to test nozzles may decrease time consumption and expenses in the nozzle design process. The small nozzle size which causes problems in the manufacturing is an advantage in CFD due to the small Reynolds numbers. The aim of this thesis is to present the basic theory involved in the design and testing of Laval nozzles and to explain some basic aspects of laser cutting processes.

Chapter 2 presents the mathematical background of using partial differential equations for modeling of physical problems. Chapter 3 explains the fundamental theory behind lasers and gives insight to the laser processes. Chapter 4 presents the theory needed for modeling of an assist gas flow and designing a Laval nozzle. Chapter 5 presents numerical methods for solving the theory presented in the Chapter 4 and a brief error analysis of these methods. Chapter 6 explains the simulation setup used in this thesis and Chapter 8 presents conclusions of this thesis.

Chapter 2

Partial differential equations

2.1 Basic concepts

This section introduces the concepts of functions, operators and most importantly weak derivatives. Weak derivatives are particularly interesting since solutions of fluid dynamics may not be continuous, for instance due to shock waves. At first it is necessary to introduce a few familiar function classes.

Definition 2.1. Let $\Omega \subset \mathbb{R}^n$. Define $C(\Omega)$ to be the set of all continuous functions from Ω to $\mathbb{R}$.

In next four definitions functions are assumed to be mappings in $\mathbb{R}$.

Definition 2.2. Let $\Omega \subset \mathbb{R}^n$. We define

$$C_0(\Omega) = \{f\colon \text{ support of } f \text{ is compact.}\} \cap C(\Omega).$$

In definition 2.2 $C_0(\Omega)$ is the set of all continuous functions that have compact (closed and bounded in $\mathbb{R}^n$) support (the set of values where $f(\mathbf{x}) \neq 0$). It is convenient to define the multi-index $\alpha = [\alpha_1, \ldots, \alpha_n] \in \mathbb{N}^n$ and the derivative

$$D^\alpha f = \Pi_{i=1}^n \frac{\partial^{\alpha_i}}{\partial x_i^{\alpha_i}} f. \tag{2.1}$$

The order of derivative D^α is given by sum

$$|\alpha| = \sum_{i=1}^{n} \alpha_i. \tag{2.2}$$

Definition 2.3. Let $\Omega \subset \mathbb{R}^n$. We define $C^m(\Omega)$ to be the set of all functions in Ω that have continuous partial derivatives of order m.

It is clear from Definition 2.3 that if a function has continuous partial derivatives of order m then all lower order derivatives must also be continuous. Let $C_0^m(\Omega)$ denote the set of all functions that have compact support and continuous derivatives of order m. Another important class of function are the locally integrable functions.

Definition 2.4. Let $\Omega \subset \mathbb{R}^n$. Now $L^p_{\text{loc}}(\Omega)$ is the set of functions f that have an integral[1]

$$\int_\Omega |f(\mathbf{x})|^p dV.$$

The next lemma is crucial for definition of weak derivatives.

Lemma 2.5. *Let $\Omega \subset \mathbb{R}^n$ and $f, g \in C_0^\infty(\Omega)$ then*

$$\int_\Omega \frac{\partial f}{\partial x_i} g dV = \int_{\partial\Omega} fg(\mathbf{e}_i^T d\mathbf{S}) - \int_\Omega f \frac{\partial g}{\partial x_i} dV,$$

where e_i is the i:th coordinate unit vector and $d\mathbf{S}$ is the outward normal differential of the surface $\partial\Omega$.

Proof. Proof can be found in [4]. □

In particular if g vanishes in $\partial\Omega$, lemma 2.5 implies that

$$\int_\Omega \frac{\partial f}{\partial x_i} g dV = -\int_\Omega f \frac{\partial g}{\partial x_i} dV. \tag{2.3}$$

Now we can postulate the definition of a weak derivative

Definition 2.6. Let $\Omega \subset \mathbb{R}^n$ and $f \in L^1_{\text{loc}}(\Omega)$. Function $(\frac{\partial f}{\partial x_i})_{\text{weak}} \in L^1_{\text{loc}}(\Omega)$ is a weak derivative of the function f iff

$$\int_\Omega \left(\frac{\partial f}{\partial x_i}\right)_{\text{weak}} \phi dV = -\int_\Omega f \frac{\partial \phi}{\partial x_i} dV \text{ , for all } \phi \in C_0^\infty(\Omega).$$

[1] Integratability is assumed to be in the Lebesque sense. However in a physical problem functions usually have an integral also in the Riemann sense.

It should be clear from Equation (2.3) that if $f \in C_0^1(\Omega)$ then its weak derivative is simply $\frac{\partial f}{\partial x_i}$. Moreover weak derivatives allow derivatives of functions to have jumps. This is an especially desirable feature in modelling problems, where the models are partial differential equations (PDE's), but the solutions might have discontinueties. From this point on the subscript "weak" will be dropped and derivatives are assumed to be weak derivatives. As we are mainly interested in those functions in $L^1_{\text{loc}}(\Omega)$ that have weak partial derivatives we need to define a new set, namely the Sobolov space [22].

Definition 2.7. Sobolov space $W^{k,p}(\Omega)$ is given by

$$W^{k,p}(\Omega) = \{f \in L^p_{\text{loc}}(\Omega) \colon D^\alpha f \in L^p_{\text{loc}}(\Omega) \text{ for all } |\alpha| \leq k\}.$$

We proceed in our discussion to operators. Operators are mappings from functions to functions. For instace derivation is an operator, but integration is not (it is a functional). We define inner product of two functions to be

$$\langle f, g \rangle = \int_{\mathbb{R}^n} f g d\mathbf{x}. \tag{2.4}$$

The inner product defined in Equation (2.4) is indeed an inner product in $W^{k,p}(\Omega)$ and proof of this can be found in [10]. The norm of a function is given by

$$\|f\| = \sqrt{\langle f, f \rangle}. \tag{2.5}$$

Continuity of an operator is defined in a similar fashion as it is for functions, as follows.

Definition 2.8. An operator T is said to be continuous iff for all f and g

$$\|f - g\| \to 0 \Rightarrow \|T(f) - T(g)\| \to 0.$$

Moreover we define addition and multiplication for operators, which are given by the following definitions.

Definition 2.9. Let T and L be operators. A sum operator $T + L$ is given by

$$(T + L)(f) = T(f) + L(f).$$

Definition 2.10. The product of operators T and L is given by

$$(TL)(f) = T(L(f)).$$

It should be noted that in definitions 2.9 and 2.10 the operators' domains and codomains must be the same and $f, g \in W^{k,p}(\Omega)$ must hold. Moreover addition is clearly commutative, but multiplication might not be.

As our main interest is in solving PDEs we are interested in differential operators. A differential operator (DO) can be defined using the following recursive rule.

Definition 2.11. Let $\Omega \subset \mathbb{R}^n$ and assume that Ω is compact. The set of differential operators Γ is given by

$$\Gamma = \cap\Gamma',$$

where the set Γ' is defined by the following rules.

1. Operator $\mathscr{L}(f) = \phi(f)$ is in Γ' for every $\phi \in C(\mathbb{R})$.
2. Operator $\mathscr{L}(f) = \frac{\partial f}{\partial x_i}$ is in Γ'.
3. If operators $\mathscr{L}$ and $\mathscr{T}$ are in Γ' then $\mathscr{L} + \mathscr{T}$ is in Γ'.
4. If operators $\mathscr{L}$ and $\mathscr{T}$ are in Γ' then $\mathscr{L}\mathscr{T}$ is in Γ'.

To show that an operator as defined in 2.11 is continuous we need following lemmas.

Lemma 2.12. *If $\mathscr{L}(f) = \phi(f)$, where $\phi \in C_0(\mathbb{R})$ then $\mathscr{L}$ is continuous.*

Proof. In this proof we need concept of essential suppremum. It represents a functions supremum in nonzero metric sets thus disregarding any solitary peaks. Let $f \in W^{k,p}(\Omega)$ and define sets

$$M_a = \{\mathbf{x} \colon f(\mathbf{x}) > a\} \text{ and}$$

$$A = \{a \colon \int_{M_a} d\mathbf{x} = 0\}.$$

The essential supremum of a function is given by [8]

$$\text{ess sup} f = \begin{cases} \infty \text{ , if } A = \emptyset \\ \inf A \text{ , otherwise} \end{cases}$$

Suppose that $\|f-g\| \to 0$. Now

$$\begin{aligned}\|\mathscr{L}(f)-\mathscr{L}(g)\|^2 &= \|\phi(f)-\phi(g)\|^2 = \int \|\phi(f)-\phi(g)\|^2 d\mathbf{x} \\ &\leq \int \text{ess sup}_{\mathbf{x}} \|\phi(f)-\phi(g)\|^2 d\mathbf{x} \\ &\leq \text{ess sup}_{\mathbf{x}} \|\phi(f(\mathbf{x}))-\phi(g(\mathbf{x}))\|^2 \text{vol}(\Omega) \to 0,\end{aligned}$$

because the essential supremums of f and g have to approach each other as $\|f-g\| \to 0$ and ϕ is continuous function in $\mathbb{R}$.

□

Lemma 2.13. *If $\mathscr{L}(f) = \frac{\partial f}{\partial x_i}$ then $\mathscr{L}$ is continuous.*

Proof. More general proof for arbitrary order derivatives can be found in [19]. □

Lemma 2.14. *If $\mathscr{L}$ and $\mathscr{T}$ are continuous then $\mathscr{L}+\mathscr{T}$ is continuous.*

Proof. Proof is of the same form as for the real valued functions. That proof can be found in any basic calculus books such as [18]. □

Lemma 2.15. *If $\mathscr{L}$ and $\mathscr{T}$ are continuous then $\mathscr{L}\mathscr{T}$ is continuous.*

Proof. Proof is of the same form as for the real valued functions. That proof can be found in any basic calculus books such as [18]. □

Now we can prove that differential operators as defined by 2.11 are continuous.

Theorem 2.16. *Differential operators as defined in 2.11 are continuous.*

Proof. Define the DO number as the minimum number of applied rules of definition 2.11 to acquire DO. For instance the DO number of $\mathscr{L} = \frac{\partial}{\partial x_i}$ is 1 and the DO number of $\mathscr{L}(f) = (\frac{\partial}{\partial x_i})^2$ is 3 (one for rule 1, one for rule 2 and one for rule 4).

Define the set $\Gamma_N = \{\mathscr{L} \in \Gamma : \mathscr{L} \text{ is not continuous }\}$. Moreover let $\mathscr{L} \in \Gamma_N$ be the DO with the lowest DO number. A type of a differential operator is defined as the last rule that is used in acquiring it.

If $\mathscr{L}$ is of type one or two it leads to contradiction with lemmas 2.12 and 2.13. Moreover if it is of type three then $\mathscr{L} = \mathscr{L}_1 + \mathscr{L}_2$. On the other hand $\mathscr{L}_i \notin \Gamma_N$ because $\mathscr{L}$ has the lowest number. This implies that $\mathscr{L}$ has to be continuous by lemma 2.14 and leads to a contradiction. Similarly if $\mathscr{L}$ is of type four then $\mathscr{L} = \mathscr{L}_1\mathscr{L}_2$. Moreover $\mathscr{L}_i$ has to be continuous by a similar argument which leads to a contradiction by lemma 2.15. Thus $\Gamma_N = \emptyset$ and all differential operators are continuous. □

Now a PDE is the equation $\mathscr{L}(f) = 0$, where the DO $\mathscr{L}$ is known. However fluid flow is modelled using multiple PDEs not a single one. Thus we need to generalize our definition to accommodate multiple unknown functions and multiple PDE's. First we define a single DO (semi generalized differential operator) with multiple unknown functions and at last multiple DOs with multiple unknown functions.

Definition 2.17. Let $\Omega \subset \mathbb{R}^n$ and assume that Ω is compact. Define the set of semi generalized differential operators (SGDO) Γ^m by

$$\begin{aligned}\Gamma^m = \{\mathscr{L} \quad : \quad & \mathscr{L}(\mathbf{f}) = \phi(\mathscr{L}_1(f_1), \ldots, \mathscr{L}_m(f_m)),\\ & \text{where } \mathbf{f} = [f_1, \ldots, f_m] \in W^{k,p}(\Omega)^m,\\ & \phi \in C(\mathbb{R}^m) \text{ and } \mathscr{L}_i \in \Gamma\}.\end{aligned}$$

Here the powers imply the cartesian set product, for instance
$W^{k,p}(\Omega)^m = W^{k,p}(\Omega)\times\cdots\times W^{k,p}(\Omega)$. Now the generalized differential operator (GDO) is given by

Definition 2.18. Let $\Omega \subset \mathbb{R}^n$ and assume that Ω is compact. Define set of generalized differential operators (GDO) $\Gamma^{m,q}$ by

$$\Gamma^{m,q} = \{\mathscr{L} \colon \mathscr{L}(\mathbf{f}) = [\mathscr{L}_1(\mathbf{f}), \ldots, \mathscr{L}_q(\mathbf{f})], \text{where } \mathscr{L}_i \in \Gamma^m\}.$$

In particular $\Gamma^{m,1} = \Gamma^m$. A PDE system can now be defined as equation $\mathscr{L}(\mathbf{f}) = \mathbf{0}$, where $\mathscr{L} \in \Gamma^{m,q}$ is known. Moreover to restrict the PDE problem to have an unique solution we need to add boundary constraints. This is usually done by demanding that functions must have a certain value at the boundary, for instance

$$\begin{aligned}&\mathscr{L}(\mathbf{f}) = \mathbf{0} \text{ such that}\\ &\mathbf{f} \in W^{k,p}(\Omega)^m \cap \{\mathbf{f} \colon \mathbf{f}(\mathbf{x}) = \mathbf{0} \text{ for all } \mathbf{x} \in \partial\Omega\}.\end{aligned}$$

2.2 Introduction to FVM

2.2.1 Variation form

Suppose that we are interested in solving the PDE $\mathscr{L}(\mathbf{f}) = \mathbf{0}$, where $\mathscr{L} \in \Gamma^{m,q}$, $\mathbf{f} \in W^{k,p}(\Omega)^m$ and $\mathbf{f}$ satisfies some boundary conditions, say $\mathbf{f}(\mathbf{x}) = \mathbf{0}$ when $\mathbf{x} \in \partial\Omega$. Then

$$\int_\Omega \|\mathscr{L}(\mathbf{f})\|^2 d\mathbf{x} \geq 0 \text{ for all } \mathbf{f} \tag{2.6}$$

In particular if $\mathbf{f}$ is the solution of the PDE then

$$\int_\Omega \|\mathscr{L}(\mathbf{f})\|^2 d\mathbf{x} = 0. \tag{2.7}$$

Thus the solution of the PDE $\mathbf{f}^*$ is given by

$$\begin{aligned} \mathbf{f}^* &= \operatorname{argmin} \int_\Omega \|\mathscr{L}(\mathbf{f})\|^2 d\mathbf{x} \text{ such that} \\ &\quad \mathbf{f} \in W^{k,p}(\Omega)^m \text{ and } \mathbf{f}(\mathbf{x}) = \mathbf{0} \text{ when } \mathbf{x} \in \partial\Omega. \end{aligned}$$

This is generally known as the variation principle. It is possible to solve the optimization problem directly using the calculus of variations which leads back to the original PDE.

Let $\mathbf{N} \in W^{k,p}(\Omega)^{m \times N}$ be known tensor. Now estimate $\mathbf{f}$ by $\hat{\mathbf{f}}$ using

$$\mathbf{f} \approx \hat{\mathbf{f}} = \mathbf{NC}, \text{where } \mathbf{C} \in \mathbb{R}^N. \tag{2.8}$$

This estimation procedure is known as the Rayleigh-Ritz method [13]. The unknown vector $\mathbf{C}$ is called the *generalized coordinates*. Using the basic theory of optimization we obtain

$$\frac{d}{d\mathbf{C}} \int_\Omega \|\mathscr{L}(\mathbf{NC})\|^2 d\mathbf{x} = \mathbf{0}. \tag{2.9}$$

2.2.2 Method of weighted residuals

The weakness of the variation form is that evaluation of $\|\mathscr{L}(\mathbf{f})\|^2$ is necessary. Moreover a result of Rayleigh-Ritz estimation does not usually satisfy the PDE. Another approach to solving PDEs numerically is to introduce the weight function ω and reguire that

$$\int_\Omega \omega_j \mathscr{L}(\hat{\mathbf{f}}) d\mathbf{x} = \mathbf{0}, \text{ for all } \omega_j \tag{2.10}$$

This is a very general technique to change PDEs to the so called integral form. Different choices of weight functions lead to different numerical methods [13]. Suppose that we have some partition of Ω, say $\{\Omega\}_{i=0}^{M}$. Now the Finite Volume Method (FVM) is acquired by choosing the following weight function

$$\omega_j(x) = \begin{cases} 1 \text{ , if } \mathbf{x} \in \Omega_j \\ 0 \text{ , otherwise} \end{cases}$$

With this weight function we try to satisfy the integral form of the PDE in each part of the partition independently. However this alone does not lead to any practical method for solving PDE's [13].

2.2.3 Fluxes

The main idea of FVM is to change a PDE to the integral form and to divide the domain to small parts (volumes). Moreover volume integrals are changed to surface integrals by introducing concept of flux. Then the parts are connected by requiring that fluxes of the neighboring parts have to be of the same order [13].

Definition 2.19. Let $\Omega \subset \mathbb{R}$ and $\mathbf{f} \in W^{k,p}(\Omega)^m$. Then tensor $\mathbf{\Phi} \in W^{k,p}(\Omega)^{m \times n}$ is flux of the function $\mathbf{f}$ iff

$$\mathbf{f} = \nabla \cdot \mathbf{\Phi}.$$

Divergence in the definition 2.19 is taken row wise. The flux of definition 2.19 is not clearly unique. Moreover the function $\mathbf{f}$ might not have a flux. However as our interest lies in fluid dynamics we don't need to discuss existence of fluxes in general as they are well known for properties of fluid dynamics. We also demostrate how some fluxes are

acquired for second order PDEs in section 2.3. To change volume integrals to surface integrals we need the divergence theorem:

Theorem 2.20. *Let* $\mathbf{\Phi} \in W^{k,p}(\Omega)^{m\times n}$ *then*

$$\int_\Omega \nabla \cdot \mathbf{\Phi} d\mathbf{x} = \int_{\partial\Omega} \mathbf{\Phi} \cdot d\mathbf{S}.$$

The dot product and divergence in theorem 2.20 are taken row wise. Now invoking the divergence theorem 2.20 to equation (2.10) and assuming that $\mathscr{L}(\hat{\mathbf{f}})$ has a flux $\mathbf{\Phi}$ we obtain

$$\begin{aligned}\int_\Omega \omega_j \mathscr{L}(\hat{\mathbf{f}}) d\mathbf{x} &= \int_{\Omega_j} \nabla \cdot \mathbf{\Phi} d\mathbf{x} \\ &= \int_{\partial\Omega_j} \mathbf{\Phi} \cdot d\mathbf{S} = \mathbf{0}.\end{aligned}$$

Note first of all that $\mathscr{L}$ has dissapeared. Moreover as fluxes are surface specific, opposing surfaces must have same fluxes with opposite directions. This leads to the FVM discretization of PDEs and is the base for further development of the method. The actual estimation of fluxes can be performed in many ways. The method used in this work is explained in chapter 6. Moreover a partition is usually called a mesh. There are many possible techniques to generate a mesh and we will explain the ones used in this work in chapter 5. Meshes are usually polygonal partitions as surface sizes of polygons are easy to evaluate [13].

2.3 Second order PDEs

This section introduces the concepts of hyberbolic, elliptic and parabolic PDEs [2, 9]. We also derive some of the most important propeties of these PDEs.

The order of a differential operator $\mathcal{L}$ is the highest order derivative present in the operator. For instance the Laplace operator ∇^2 is a second order operator. Differential equations $\mathcal{L}(f) = 0$, where the $\mathcal{L}$ is a second order operator are called second order PDEs. The general form of second order PDE can be given as

$$\sum_{i,j=1}^{n} A_{ij} \frac{\partial^2}{\partial x_i \partial x_j} f + \sum_{i=1}^{n} B_i \frac{\partial}{\partial x_i} f + Cf = g, \tag{2.11}$$

where A_{ij} are constant, B_i and C are functions of x; f and g are known functions of x. Consider a change of coordinates from $x \in \mathbb{R}^n$ to $\xi \in \mathbb{R}^n$. In order to be a proper change of variables the Jacobian $\frac{dx}{d\xi}$ must be invertible.

If we let $\xi = Fx$, where $F \in \mathbb{R}^{n\times n}$, then the Jacobian is $\frac{d\xi}{dx} = F$ and we require that the matrix F should be invertible.

Due to the change of coordinates we have

$$\begin{aligned}\frac{\partial}{\partial x_i} &= \sum_{j=1}^{n} \frac{\partial \xi_j}{\partial x_i}\frac{\partial}{\partial \xi_j} \\ &= \sum_{j=1}^{n} F_{ij}\frac{\partial}{\partial \xi_j}.\end{aligned}$$

Thus in the coordinates ξ the PDE (2.11) takes the form

$$\sum_{i,j=1}^{n} A_{ij}\chi_{ij}\frac{\partial^2}{\partial \xi_i \partial \xi_j} f + \cdots = g, \tag{2.12}$$

where χ_{ij} is given by

$$\begin{aligned}\chi_{ij} &= \sum_{k,l=1}^{n} A_{kl}\frac{\partial \xi_i}{\partial x_k}\frac{\partial \xi_j}{\partial x_l} \\ &= \sum_{k,l=1}^{n} A_{kl}F_{ik}F_{jl}.\end{aligned}$$

Now we would like to have $\chi_{ij} = 0$ for all $i \neq j$, which would transform equation (2.11) to the so called canonical form. In general this is not possible, but if A_{ij} are constants then we will be able to obtain the canonical form. Moreover χ can be given in the matrix form

$$\chi = FAF^T. \tag{2.13}$$

Since differentiation is assocative, the matrix A can always be required to be symmetric. Schur decomposition is given in following theorem.

Theorem 2.21. *Let $A \in \mathbb{R}^{n\times n}$ then there exists an unitary matrix Q and an upper triangular matrix Λ such that*

$$A = Q\Lambda Q^*.$$

Proof. Proof can be found in [5]. □

For symmetric real matrices

$$\begin{aligned} A &= Q\Lambda Q^T \\ &= A^T = (Q\Lambda Q^T)^T = Q\Lambda^T Q^T. \end{aligned}$$

Thus $\Lambda^T = \Lambda$. Since Λ is always upper triangular it follows that for symmetric matrices A it reduces to a diagonal matrix. Diagonal elements of Λ are the eigenvalues λ_i of A.

If all eigenvalues in equation (2.11) have same sign (i.e they are all positive or negative) the equation is called elliptic. If one or two eigenvalues have a different sign from rest of eigenvalues then equation is called normal hyberbolic or ultra hyberbolic, respectively. Ultra hyberbolic equations do not arise in a natural way in mathematical physics and will not be discussed in more detail. If one or more eigenvalues are zero then equation is called parabolic.

Definition 2.22. Let $\Omega \in \mathbb{R}^n$ and $\xi \in C^1(\Omega)$. The characteristic surface $\mathcal{S}_\beta$ of ξ is defined as

$$\mathcal{S}_\beta = \{\mathbf{x} \in \mathbb{R}^n \colon \xi(\mathbf{x}) = \beta\}. \tag{2.14}$$

It should be noted that ξ in definition 2.22 presents a single coordinate. In linear case $\xi = F\mathbf{x}$ we have $\xi_i = F_i\mathbf{x} = \beta$. Thus characteristic surfaces are hyperplanes. However in the nonlinear case characteristic curves might not be hyperplanes. If we limit our attention to a single characteristic surface, say coordinate ξ_i is held constant and the corresponding surface is $\mathcal{S}_\beta$ we have

$$\chi_{ii} = \sum_{k,l=1}^{n} \frac{\partial \xi_i}{\partial x_k}\frac{\partial \xi_i}{\partial x_l} = 0, \text{ for all } \mathbf{x} \in \mathcal{S}_\beta. \tag{2.15}$$

Hence if we solve a PDE on the characteristic curve one of the second order derivatives vanishes. In particular this is interesting in case of two variables, where it transforms a

PDE to an ODE (ordinary differential equation). In next sections we introduce fluxes arising from these types of equations.

2.3.1 Hyperbolic PDEs

In this section we discuss hyberbolic PDEs. We limit our discussion to normal hyperbolic equations and omit ultra hyberbolic equations as they are not of great interest. One of the most important hyberbolic equations is the (linear) wave equation given by

$$\frac{\partial^2 f}{\partial t^2} - c_0^2 \nabla^2 f = 0, \tag{2.16}$$

where c_0 is a constant called the speed of the wave. For electromagnetic radiation it is the speed of light and for sound waves it is the speed of sound [7].

Recall the canonical form of hyberbolic PDE

$$\sum_{i=1}^{n} \lambda_i \frac{\partial^2 f}{\partial x_i^2} + \cdots = \frac{\partial^2 f}{\partial t^2}, \tag{2.17}$$

where the ellipeses $\cdots$ represents the lower order derivative terms, t is used to denote derivatives with a different sign and $\lambda_i > 0$ due to definition of hyberbolic equations. We introduce a new vector valued function $\mathbf{u} \in W^{k,p}(\Omega)^n$ and $v \in W^{k,p}(\Omega)$. We require that

$$u_i = \frac{\partial f}{\partial x_i} \text{ and} \tag{2.18}$$

$$v = \frac{\partial f}{\partial t}. \tag{2.19}$$

Now the canonical form is changed to

$$\sum_{i=1}^{n} \lambda_i \frac{\partial u_i}{\partial x_i} + \cdots = \frac{\partial v}{\partial t}, \tag{2.20}$$

which is a first order PDE system. A PDE system acquired from a hyberbolic second order equation is called hyperbolic system.

Using divergence $\nabla\cdot$ we may write equation (2.20) as

$$\nabla \cdot (\Lambda \mathbf{u}) \cdots = \frac{\partial v}{\partial t}. \tag{2.21}$$

Integrating both sides of the equation (2.21) over Ω yields

$$\int_\Omega \nabla \cdot (\Lambda \mathbf{u})\, d\mathbf{x} + \cdots = \int_\Omega \frac{\partial v}{\partial t} d\mathbf{x}. \tag{2.22}$$

Invoking the divergence theorem 2.20 on the left side we obtain

$$\int_{\partial\Omega} \Lambda \mathbf{u} \cdot d\mathbf{S} + \cdots = \frac{\partial}{\partial t} \int_\Omega v d\mathbf{x}. \tag{2.23}$$

Equation (2.23) is known as the hyperbolic conservation law and is of great importance when solving hyperbolic equations by FVM due to the presence of the flux $\Lambda\mathbf{u}$ [2, 9, 15].

2.3.2 Elliptic PDEs

Elliptic PDEs are usually involved in field problems, where fields have a so called scalar potential. Most common elliptic PDE is the Laplace equation given by $\nabla^2 f = 0$. This equation arises for instance in electrostatics and in steady potential flow (incompressible and irrotational flow) [10].

The canonical form of an elliptic equation is given by

$$\sum_{i=1}^{n} \lambda_i \frac{\partial^2 f}{\partial x_i^2} + \cdots = 0. \tag{2.24}$$

Introducing a new vector valued function $\mathbf{u} \in W^{k,p}(\Omega)^n$ and requiring that

$$u_i = \frac{\partial f}{\partial x_i}, \tag{2.25}$$

we may change an elliptic equation to

$$\sum_{i=1}^{n} \lambda_i \frac{\partial u_i}{\partial x_i} + \cdots = 0. \tag{2.26}$$

Integrating equation (2.26) over Ω and invoking the divergence theorem we obtain

$$\int_{\partial\Omega} \Lambda \mathbf{u} \cdot d\mathbf{S} + \cdots = 0. \tag{2.27}$$

In absence of other than flux terms we have

$$\int_{\partial\Omega} \Lambda \mathbf{u} \cdot d\mathbf{S} = 0. \tag{2.28}$$

Equation (2.28) is a conservation principle for elliptic equations with only second order terms "everything that comes in has to come out" and there is "no storing of stuff".

2.3.3 Parabolic PDEs

One of the best known parabolic equations is the heat equation $\frac{\partial f}{\partial t} = k\nabla^2 f$. Since parabolic equations may appear in many forms we consider only following equation similar to the heat equation

$$\sum_{i=0}^{n} \lambda_i \frac{\partial^2 f}{\partial x_i^2} = \frac{\partial f}{\partial t}. \tag{2.29}$$

Again introducing a new vector valued function $\mathbf{u} = \nabla f$ we have

$$\nabla \cdot (\Lambda \mathbf{u}) = \frac{\partial f}{\partial t}. \tag{2.30}$$

Integrating and invoking the divergence theorem we obtain

$$\int_{\partial\Omega} \Lambda \mathbf{u} \cdot d\mathbf{S} = \frac{\partial}{\partial t} \int_{\Omega} f d\mathbf{x}. \tag{2.31}$$

Equation (2.31) is similar to the one in the case of hyperbolic functions. However if there are no first order terms in the original canonical form then the right hand side of equation (2.31) would be zero in a similar way to equation (2.28) [9].

Chapter 3

Principles of laser cutting

3.1 Electromagnetic radiation

3.1.1 General features

Lasers consist of electromagnetic radiation. Electromagnetic radiation can be explained by two distinct theories. The first one states that electromagnetic radiation is a fluctuating wave of electric and magnetic fields through space. The second model states that electromagnetic radiation is a flow of particles called photons. The propagation speed of electromagnetic radiation is always the speed of light c. Both theories explain different aspects of radiation, and it can be said that electromagnetic radiation has a dual nature.

The fundamental properties of radiation are its wavelength λ and frequency f. Frequency and wavelength are connected by the equation (3.1)

$$\lambda f = c. \tag{3.1}$$

In the photon theory the momentum p of a single photon is given by

$$p = \frac{h}{\lambda}, \tag{3.2}$$

where $h = 6.625 \times 10^{-34}$Js is Planck's constant. The energy of a single photon is given by

$$E = hf. \tag{3.3}$$

Recall the famous Maxwell equations for electric and magnetic fields in a vacuum, which are given by

$$\nabla \cdot \mathbf{E} = 0, \tag{3.4}$$
$$\nabla \cdot \mathbf{B} = 0, \tag{3.5}$$
$$\nabla \times \mathbf{E} = -\frac{\partial \mathbf{B}}{\partial t} \text{ and} \tag{3.6}$$
$$\nabla \times \mathbf{B} = \mu_0 \epsilon_0 \frac{\partial \mathbf{E}}{\partial t}. \tag{3.7}$$

To obtain a wave equation for $\mathbf{E}$ and $\mathbf{B}$ we need following lemma.

Lemma 3.1. *For $\mathbf{f} \in W^{p,q}(\Omega)^3$ the following identity holds:*

$$\nabla \times \nabla \times \mathbf{f} = \nabla (\nabla \cdot \mathbf{f}) - \nabla^2 \mathbf{f}.$$

Proof. Let $\mathbf{f} = [u, v, h]^T$. Also use the standard coordinate vectors $\mathbf{i}$, $\mathbf{j}$ and $\mathbf{k}$ to simplify notation. Now expanding the left side we obtain

$$\begin{aligned}
\nabla \times \nabla \times \mathbf{f} &= \left(-\frac{\partial^2 u}{\partial z^2} + \frac{\partial^2 h}{\partial x \partial z} - \frac{\partial^2 u}{\partial y^2} + \frac{\partial^2 v}{\partial x \partial y}\right)\mathbf{i} \\
&\quad + \left(-\frac{\partial^2 v}{\partial z^2} + \frac{\partial^2 h}{\partial y \partial z} - \frac{\partial^2 u}{\partial x \partial y} + \frac{\partial^2 v}{\partial y^2}\right)\mathbf{j} \\
&\quad + \left(\frac{\partial^2 v}{\partial y \partial z} - \frac{\partial^2 h}{\partial y^2} + \frac{\partial^2 u}{\partial x \partial z} - \frac{\partial^2 h}{\partial x^2}\right)\mathbf{k} \\
&= \left(\frac{\partial^2 u}{\partial x^2} + \frac{\partial^2 v}{\partial x \partial y} + \frac{\partial^2 h}{\partial x \partial z}\right)\mathbf{i} - \left(\frac{\partial^2 u}{\partial x^2} + \frac{\partial^2 u}{\partial y^2} + \frac{\partial^2 u}{\partial z^2}\right)\mathbf{i} \\
&\quad + \left(\frac{\partial^2 u}{\partial x \partial y} + \frac{\partial^2 v}{\partial y^2} + \frac{\partial^2 h}{\partial y \partial z}\right)\mathbf{j} - \left(\frac{\partial^2 v}{\partial x^2} + \frac{\partial^2 v}{\partial y^2} + \frac{\partial^2 v}{\partial z^2}\right)\mathbf{j} \\
&\quad + \left(\frac{\partial^2 u}{\partial x \partial z} + \frac{\partial^2 v}{\partial y \partial z} + \frac{\partial^2 h}{\partial z^2}\right)\mathbf{k} - \left(\frac{\partial^2 h}{\partial x^2} + \frac{\partial^2 h}{\partial y^2} + \frac{\partial^2 h}{\partial z^2}\right)\mathbf{k} \\
&= \nabla (\nabla \cdot \mathbf{f}) - \nabla^2 \mathbf{f}.
\end{aligned}$$

□

Invoking lemma 3.1 we may write

$$\begin{aligned} \nabla \times \nabla \times \mathbf{E} &= -\nabla \times \frac{\partial \mathbf{B}}{\partial t} \\ &= \nabla (\nabla \cdot \mathbf{E}) - \nabla^2 \mathbf{E} = -\nabla^2 \mathbf{E}. \end{aligned}$$

Moreover the magnetic field can be simplified further by Maxwell's laws to yield

$$\nabla \times \frac{\partial \mathbf{B}}{\partial t} = \frac{\partial}{\partial t} (\nabla \times \mathbf{B}) = \mu_0 \epsilon_0 \frac{\partial^2 \mathbf{E}}{\partial t^2}.$$

Combining equations we may write

$$\mu_0 \epsilon_0 \frac{\partial^2 \mathbf{E}}{\partial t^2} = \nabla^2 \mathbf{E}. \tag{3.8}$$

Similarly for magnetic field

$$\mu_0 \epsilon_0 \frac{\partial^2 \mathbf{B}}{\partial t^2} = \nabla^2 \mathbf{B}. \tag{3.9}$$

Thus $\mathbf{E}$ and $\mathbf{B}$ satisfy the wave equation. The general solution for equations (3.8) and (3.9) is $\mathbf{E} = \hat{\mathbf{E}} g(\mathbf{k} \cdot \mathbf{x} - ct)$, where $\hat{\mathbf{E}}$ is called amplitude, $c = (\mu_0 \epsilon_0)^{-1/2}$ and g is an arbritary continuous function. Moreover $\mathbf{B} = \frac{1}{c} k \times \mathbf{E}$.

If two or more waves overlap they interfere with each other. The new wave created by interference is a linear combination of interfering waves. If waves have the same frequency then interference can be constructive or destructive. Interference is constructive if waves are in same phase and destructive if they are in opposite phases. Destructive interference causes wave front to diminish and constructive interference amplitude to grow larger.

Moreover in an electromagnetic wave each point of the wave front acts as a new wave source. This is known as the Huygens principle [20, 6].

3.1.2 Interaction with matter

Matter consists of atoms. Atoms consists of a nucleus and an electron cloud. Electrons exist in various discrete energy states. Thus there is only a numerable set of energy

states in which electrons may exist. When an electron absorbs energy it is excited to an upper energy state. An excited electron may emit a photon and move to a lower energy state. Due to conservation of energy, the energy of an emitted photon has to be equal to the difference of the electron's initial and final energy states. Similarly an electron may absorb a photon and move to a higher energy state.

When radiation strikes matter it may be reflected, refracted, absorbed or scatered. The specific forms of interaction depends highly on the wavelength of the radiation and the phase and quality of the matter [20].

3.2 Lasers

3.2.1 Operation principle

Laser technology is based on the principle of stimulated emission. Suppose a scheme where we have matter which is exposed to electromagnetic radiation. The matter's electrons can exist in a lower or an upper energy state. The upper energy state is called excited state. Let N_2 be the number of electrons in the upper excited state and the N_1 the number of electrons in the lower energy state.

As explained in section 3.1.2 excited electrons may emit photons at frequency f given by the energy difference of the lower and upper energy states. However, if an excited electron is disturbed by electromagnetic radiation it will emit a photon which is in the same phase as the disturbing radiation. Thus constructive interference may occur. This phenomenon is called *stimulated emission*. The gross rate of emission is governed by the equation (3.10)

$$\frac{\partial N_2}{\partial t} = -\frac{\partial N_1}{\partial t} = -B_{21}\rho(f)N_2, \tag{3.10}$$

where B_{21} is called Einstein's B coefficient and $\rho(f)$ is the density of the frequency f. The first equality in equation (3.10) is due to conservation of the number of electrons.

Similarly the gross rate of absorption is given

$$\frac{\partial N_2}{\partial t} = -\frac{\partial N_1}{\partial t} = B_{12}\rho(f)N_1. \tag{3.11}$$

Einstein showed that for stimulated emission $B_{12} = B_{21}$. Taking into account absorption and emission of photons we obtain the net rate of emission given by

$$\frac{\partial N_1^{\text{net}}}{\partial t} = B_{12}\rho(f)\,(N_2 - N_1) = B_{12}\rho(f)\Delta N. \tag{3.12}$$

From equation (3.12) follows that a net power of $\frac{\partial N_1^{\text{net}}}{\partial t} \times hf$ is added to radiation. In order to strengthen the radiation $\Delta N > 0$. Otherwise, stimulated emission will weaken the radiation. The condition $\Delta N > 0$ is known as the *population inversion* and is a necessary condition for a laser to function. Name of laser originates from stimulated emission and is an acronym for *Light Amplification by Stimulated Emission of Radiation*.

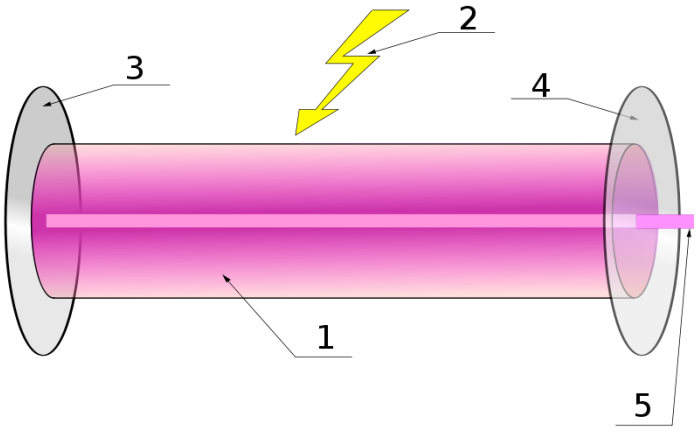

Figure 3.1: Illustration of the operation principle of laser. 1: gain medium. 2: is radiation source.3: is Reflecting mirror. 4: is partially reflecting mirror. 5: is laser beam. Picture is taken from website http://en.wikipedia.org/wiki/Laser.

An usual laser apparatus consist of two mirrors parallel to each other and a gain medium between the mirrors which has the polulation inversion property. One of the mirrors is totally reflecting and the other partially. The partially reflecting mirror is usually called the output mirror. Once electromagnetic radiation like light is supplied to the gain medium, it starts to amplify a certain frequency of electromagnetic radiation bouncing back and forth from mirrors. This amplified radiation is called the laser beam. The efficiency of a laser is given as a ratio of output laser power to total input electrical power. In this context *total* means electrical power supplied to the gain medium as well as accessories such as cooling devices.

Output mirrors (partially reflecting mirror) can be split in two classes depending how they alter the laser beam, namely *stable* and *unstable* designs. In a stable design the output mirror causes the oscillating beam to converge and in an unstable design it causes the beam to diverge. Most low power lasers use a stable design. However high power lasers usually use an unstable design to reduce thermal stress in the mirrors.

Another fundamental property of lasers is the Fresnel number N_F given by

$$N_F = \frac{R^2}{\lambda L}, \tag{3.13}$$

where R is the radius of the output mirror and L is the distance between the mirrors, also called the cavity length. The Fresnel number indicates the number of off-axis oscillations that may exist in the cavity. Therefore a low Fresnel number is desired feature of laser [20, 6].

3.2.2 Carbon Dioxide laser

Carbon dioxide lasers use carbon dioxide as a gain medium. There is typically $10\% - 20\%$ of carbon dioxide, $10\% - 20\%$ of nitrogen, few percent of hydrogen and xenon and a small amount of helium. Carbon dioxide laser has its principal wavelength at 9.4 µm - 10.6 µm. Carbon dioxide lasers are powerful and widely used lasers today. Drawback of the carbon dioxide laser is that the carbon dioxide has to be cooled. Efficiency of carbon dioxide lasers typically is only around 12% due to the requirement of cooling. Figure 3.2 shows a carbon dioxide laser.

Carbon dioxide lasers can be split in two classes depending how the cooling is achieved, namely Slow Flow Lasers (SFL), Fast Axial Flow Lasers (FAFL) and Transverse Flow Lasers (FTFL).

Figure 3.2: Example of carbon dioxide laser. This photo is taken from website http://en.wikipedia.org/wiki/Carbon_dioxide_laser.

In a slow flow lasers cooling is achieved through the walls of the gain medium by conduction. Moreover there is a maximum temperature at which lasing action can

take place. Therefore the maximum power of laser is directly connected to the cooling power supplied.

Laser gain mediums are usually cylinder symmetric. Assuming that the temperature is steady ($\frac{\partial}{\partial t} = 0$) and cylinder symmetric we may write

$$\frac{dT}{dr} = \frac{Qr}{2k}, \tag{3.14}$$

with a boundary condition on cylinder wall

$$T(R) = T_c, \tag{3.15}$$

where R is radius of gain medium.

Solving for temperature distribution from the differential equation (3.14) yields

$$T = T_c + \frac{QR^2}{4k}\left(1 - \left(\frac{r}{R}\right)^2\right). \tag{3.16}$$

The maximum temperature is obtained in the middle of the medium $r = 0$. Therefore the maximum temperature is given by

$$T_{\max} = T_c + \frac{QR^2}{4k}. \tag{3.17}$$

Denoting the maximum allowed temperature by $T_{\lim}$ we obtain a formula for cooling flow given by

$$Q = \frac{4k}{R^2}\left(T_{\lim} - T_c\right). \tag{3.18}$$

Moreover, the maximum power of laser P is connected to the heat flow Q by [20]

$$P = \eta Q\left(\pi R^2 L\right) = 4\pi k L \eta\left(T_{\lim} - T_c\right), \tag{3.19}$$

where L is the length of the gain medium cylinder and η the efficiency of the laser. In particular $P \propto L$. Usually $T_{lim} = 523\text{K}$, $T_c = 283\text{K}$ and $k = 0.14\text{WmK}^{-1}$ which gives $P/L = 50\text{W/m}$. Due to this SFLs are either weak (less than 2kW) or very long like

Essex University laser which was almost 70m. Long cavity also implies low Fresnel number.

Fast axial flow lasers achieve cooling through axial gas flow through the gain medium. Compared to SFLs, FAFLs achieve ten times greater power to length ratios, making them more suitable for compact high power lasers.

Assuming that conduction of heat is negligible compared to heat convection we may write

$$\rho C\left(T - T_c\right) = \frac{Qx}{u}, \tag{3.20}$$

where ρ is the density of gas, T_c the initial temperature of gas, x the axial position and u is the mean velocity of gas. The maximum temperature is achieved at the end of the gain medium and is given by

$$T_{\max} = T_c + \frac{QL}{\rho u C}. \tag{3.21}$$

As in the case of the SFL we obtain laser power P as

$$P = \eta A u \rho C\left(T_{\lim} - T_c\right). \tag{3.22}$$

In particular $P \propto Au$. A problem with powerful FAFLs is that the fresnel number is usually high due to

$$N_F = \frac{R^2}{\lambda L} \propto A \propto P. \tag{3.23}$$

In Transverse flow laser (FTFL) cooling is achieved with gas flow, but the flow direction is transverse to the laser beam. This allows more efficient cooling than axial flow, but FTFLs lack the flow symmetry present in FAFLs. There are also other flow patterns, which are not discussed in this thesis [20].

3.2.3 Diode laser

Diode lasers are based on semiconductors for instance GaAs and GaAlAs. The wavelength of this type of a laser depends heavily on temperature and thus cooling must be designed carefully. Diode lasers are usually used in DVD players and function as

low power lasers. They typically cannot be used directly for laser processes (cutting, welding, surface hardening etc.), but recently there have been developed some more powerful diode lasers that have enough power for the direct laser process applications. In laser processes diode lasers usually function as a pumping source for a more powerful Nd-YAG laser [20].

3.2.4 Solid State laser

Solid state lasers use a solid gain medium. The gain medium is typically a rod. The essence of this type of a laser is the process of supplying radiation into the rod and cooling of the rod.

The most widely used solid state laser is the Nd-YAG laser in which the rod consist of neodymium-doped yttrium aluminium garnet rod. Figure 3.3 shows a typical Nd-YAG rod. The wavelength of Nd-YAG lasers is typically 1064nm.

Nd-YAG lasers are typically pulsed. This means that instead of a continuous beam it produces short beam pulses with a given frequency. Frequencies of the Nd-YAG laser pulses usually range from $0 - 50$kHz. This pulsing is usually done by a device called the Q-switch or a circuit boad, which determines the pulse type. The continuous operating power of the Nd-YAG lasers range up to 5kW lasers. The powerful Nd-YAG lasers can be used for cutting purposes. Nd-YAG lasers also have better efficiency than carbon dioxide lasers at 20%.

Power can be supplied by a flash lamp or by diode lasers. Flash lamps are usually cheap, but their efficiency is not good as most of energy ends on heating the YAG rod.

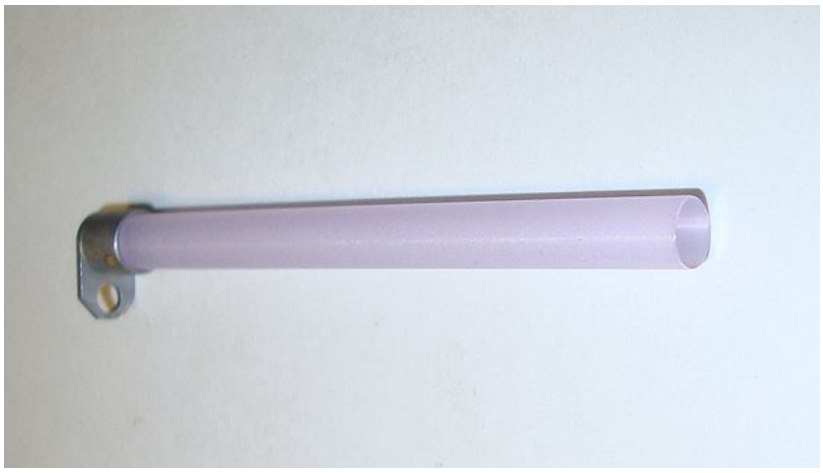

Figure 3.3: Example of Nd-YAG rod. This photo is taken from website http://en.wikipedia.org/wiki/User:Zaereth.

On the other hand, diode laser supply does not suffer from this problem, but has a larger initial cost [20].

3.3 Laser cutting techniques

3.3.1 General aspects

Laser cutting is nowadays a widely used as a manufacturing technique. Before discussing the actual advantages of laser cutting, some general aspects of metal cutting are presented.

When metal is cut there is usually a rise in temperature. The elevated temperature causes shear stresses which may affect the structure of the surrounding metal. The area of metal which is affected by this rise in temperature is called the Heat Affected Zone (HAZ). It is desirable that HAZ be as small as possible. Laser cutting generally has small HAZ due to the high energy density.

The cutting of metal is usually executed by removal of material from the cut area. The width of this cut area is called kerf. This removed material is lost and therefore adds to material expense. Hence it is desirable that the kerf be as thin as possible. The kerf of laser cutting techniques is usually narrower than traditional cutting methods, for instance plasma cutting. Laser cutting can also do very steep edges and corners without rounding them. Cut edges are also usually very clean which makes immediate welding possible.

As a process, laser cutting is highly flexible as similar lasers can be used to cut a wide variety of materials including plastics, metals and wood. Moreover, there is no tool wear because there are no contact to the material being cut.

Expenses in laser cutting consist of the initial expense of laser equipment and running expenses of electricity and assist gas, which is usually nitrogen or oxygen. The electrical expense can be high as for instance a $100kW$ carbon dioxide laser working at an efficiency of $\eta = 10\%$ requires $1MW$ of electricity [20, 6, 16].

3.3.2 Vaporisation cutting

In vaporisation cutting, the laser beam is concentrated at a single point of the surface of the metal and the metal is heated to the vaporisation point. Once metal is vaporized high velocity gas flow is concentrated at the cut point to blow vaporisated metal out of

the cut. In general cutting characteristics become better if more gas is used. However, a large amount of gas flow increases expenses. This creates a need for nozzles that improve cutting characteristics while using less gas [20].

3.3.3 Fusion cutting

Fusion cutting is similar to vaporisation cutting except metal is only melted. Molten metal is blown out of the cut using a high speed gas flow. Fusion cutting generally needs only 10% of the power needed for vaporisation cutting thus making it more economical [20].

3.3.4 Reactive fusion cutting

Reactive fusion cutting uses a high speed oxygen flow to simultaneously burn and blow away the molten metal. This method allows thicker material than fusion cutting, but introduces striations in cut. Striations are deviations in the cut wall.

The effectiveness of reactive fusion cutting depends on material being cut. For steel, heat added by burning of oxygen is usually 60 % of the power supplied by laser. However, for titanium it rises to 90%. Cutting speed of reactive fusion cutting is usually at least double compared to normal fusion cutting [20].

3.3.5 Laser assisted oxygen cutting

Laser assisted oxygen cutting, known as the LASOX process, is a variant of reactive fusion cutting where the laser is used only to ignite oxygen. The actual cutting is performed by oxygen burning the metal. This method enables very deep cuts.

In LASOX, the laser power doesn't need to be high, because cutting is achieved by chemical reactions. Required laser power is typically 1kW. Lower limit to required power is set by ignition temperature of material. For instance, steel has to be heated to $900°C - 1000°C$ in order to initiate the LASOX process. This requirement is commonly known as the LASOX condition [20].

3.4 The effects of assist gas flow

This section discusses briefly how a assist gas flow effects the cut characteristics in case of a laser cutting. Desired features of the gas flow depend on the quality and shape of material. In the case of metal cutting, dross is usually formed in the back side of the workpiece (Figure 3.4). It has been experimentally shown that the height of dross decreases when velocity of assist gas is increased.

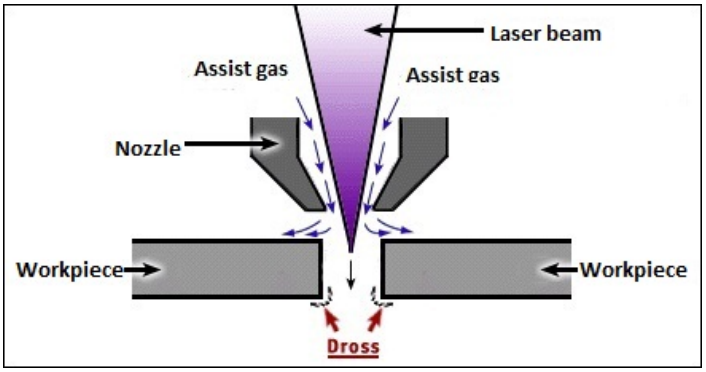

Figure 3.4: Formation of dross in the laser cutting of metal. Picture is taken from website http://www.teskolaser.com/laserglossaryd.html and modified slightly.

Given a nozzle, velocity on the workpiece can be increased by increasing the pressure of assist gas prior to the nozzle. On the other hand this technique increases costs of assist gas flow. By suitable nozzle design velocity of assist gas can be increased without increasing the inlet pressure. How this is done will be explained in chapter 4.

Chapter 4

Fluid dynamics

4.1 Thermodynamic relations

Thermodynamic relations relate thermodynamic properties such as density and temperature. The ideal gas law is given by

$$pM = \rho RT, \tag{4.1}$$

where p is pressure, M is molar mass of the gas, ρ is density, R is universal ideal gas constant and T is temperature. The ideal gas law is usually a good model for low pressure and low density gases. It is also the most widely used gas model. It will be used in this thesis even through pressures are rather large (10bar). The inverse of density ν is called the specific volume. Specific properties are properties relative to mass and are presented by small letters. For instance if U is the internal energy then specific internal energy is given by $u = U/m$. The word specific is usually dropped and both internal energies are referred to as internal energy.

The (specific) enthalpy of a gas is given by

$$h = u + p\nu, \tag{4.2}$$

where u is the (specific) internal energy. For ideal gases internal energy and enthalpy are functions of only the temperature. The temperature of a gas can increase due to an increase in pressure (mechanical work) or due to the heat addition. In the case of heat addition δQ, temperature of gas will rise amount given by

$$\delta T = \frac{1}{c}\delta Q, \tag{4.3}$$

where c is the (specific) heat capacity. The heat capacity depends on the mechanism of heat addition. For constant pressure processes the heat capacity is given by

$$c = c_p = \frac{\partial h}{\partial T}. \tag{4.4}$$

For constant volume processes the heat capacity is given by

$$c = c_V = \frac{\partial u}{\partial T}. \tag{4.5}$$

Moreover for ideal gases that obey the equation (4.1) we have

$$c_p - c_V = \frac{R}{M}. \tag{4.6}$$

Heat capacities are given by $C_V = mc_v$ and $C_p = mc_p$. Properties ρ, p and T are called state properties. Given two state variables the third one can be calculated. In particular state properties are independent from the way processes are excecuted. We define new state variable, entropy as

$$dS = (\frac{\delta Q}{T})_{\text{rev}}. \tag{4.7}$$

Subscript rev implies that integration is done along a reversible path. In particular

$$\oint dS = \oint (\frac{\delta Q}{T})_{\text{rev}} = 0. \tag{4.8}$$

For real world processes

$$\oint \frac{\delta Q}{T} \leq \oint (\frac{\delta Q}{T})_{\text{rev}} = 0. \tag{4.9}$$

Thus entropy change is positive due to

$$\frac{\delta Q}{T} - dS \leq (\frac{\delta Q}{T})_{\text{rev}} - dS = 0. \tag{4.10}$$

Thus equation (4.10) applied to a closed system yields

$$dS \geq \frac{\delta Q}{T} = 0, \tag{4.11}$$

due to $\delta Q = 0$. A process is called isentropic if $dS = 0$. In this work by an isentropic process we mean an adiabatic (no heat transfer) and reversible process. However strictly saying that a process is isentropic process does not necessarily imply that it is adiabatic and reversible. Isentropic processes conserve entropy.

Since isentropic processes are assumed to be adiabatic we have $\delta Q = 0$. Thus the internal energy is given by

$$dU = dW + \delta Q = dW = pdV, \tag{4.12}$$

where dV is the differential volume change.

Similarly enthalpy is given by

$$dH = pdV. \tag{4.13}$$

Invoking heat capacities we have

$$dU = nC_V dT \tag{4.14}$$

and

$$dH = nC_p dT. \tag{4.15}$$

Defining a constant $\gamma = C_p/C_V$ we may write

$$\frac{dH}{dU} = \gamma = -\frac{dp/p}{dV/V}. \tag{4.16}$$

The constant $\gamma = 1.4$ for diatomic ideal gases. Integrating the equation (4.16) yields

$$d\left(pV^{\gamma}\right) = 0. \tag{4.17}$$

We formulate the ideal gas law as

$$\frac{p}{\rho} = \frac{R}{M}T = \frac{R}{Mc_V}u = \frac{c_p - c_V}{c_V}u = (\gamma - 1)\, u. \tag{4.18}$$

The speed of sound c for ideal gases is given by [21]

$$c^2 = \frac{\gamma RT}{M}. \tag{4.19}$$

A flow where the flow velocity is below the speed of sound is called subsonic and supersonic if it is above the speed of sound. The limiting case in which velocity is the speed of sound is called transonic. Velocity relative to the speed of sound is called the Mach number.

In particular the Mach number is interesting in nozzle flow, because a flow shows very distinct behavior depending on wheather it is supersonic or subsonic. In addition supersonic flows may give rise to shock effects (sudden drops or rises in pressure) which cause discontinueties in solutions. These features are further explained in section 4.4 for nozzle flows.

For supersonic flows it is suitable to define stagnation properties. These properties denote what the underlying properties would be if the fluid flow were suddenly stopped. In particular stagnation pressure and temperature are given by

$$p_S = p + \frac{\rho \|\mathbf{u}\|^2}{2}, \tag{4.20}$$

where $\mathbf{u}$ is velocity and

$$T_S = T\left(1 + \frac{\gamma - 1}{2}M^2\right), \tag{4.21}$$

where M is Mach number of flow and T is (static) temperature. The name *stagnation* comes from the stagnation point which is the point where flow velocity is zero [14, 3, 17].

4.2 Conservation laws

Fluid flow is governed by the thermodynamic relations described in section 4.1 and conservation laws. Conservation laws consist of five equations. The first law, *conservation of mass* states that the mass of a system must remain constant. The Newton's

law of dynamics yield *conservation of momentum* which consists of three equations. Moreover the first law of thermodynamics states that energy cannot be created or destroyed which yields *conservation of energy* [2, 13].

4.2.1 Conservation of mass

Conservation of mass is given by

$$\frac{\partial \rho}{\partial t} + \nabla \cdot (\rho \mathbf{u}) = 0. \tag{4.22}$$

This equation states that a change of density at a point is due to a mass flux $\rho\mathbf{u}$. To simplify the notation it is custom to use the substantial derivative given by

$$\frac{D(\cdot)}{Dt} = \frac{\partial(\cdot)}{\partial t} + \mathbf{u} \cdot \nabla(\cdot). \tag{4.23}$$

The substantial derivative is also called the convective or material derivative and presents a derivative relative to a moving point rather than to a fixed point. Using this notation conservation of mass can be writen as

$$\frac{D\rho}{Dt} + \rho \nabla \cdot \mathbf{u} = 0. \tag{4.24}$$

If a fluid is incompressible such as water, the equation (4.22) can be simplified further to yield

$$\nabla \cdot \mathbf{u} = 0. \tag{4.25}$$

However equation (4.25) is not a proper model for supersonic gas flows since compressibility is major feature of these flows [2, 13].

In the steady case ($\frac{\partial}{\partial t} = 0$) it is possible to eliminate the time derivative. However in a numerical solution this is not usually done because it changes the type of equation from hyberbolic-parabolic to hyberbolic-elliptic which causes difficulties for a numerical solver. Thus steady problems are usually modelled using unsteady equations with a relatively large time step [2]. This is explained in chapter 5.

4.2.2 Conservation of momentum

Conservation of momentum can be writen as

$$\frac{\partial}{\partial t}(\rho \mathbf{u}) + \nabla \cdot (\rho \mathbf{u}\mathbf{u}) = \rho \mathbf{f} + \nabla \cdot \mathbf{\Pi}, \tag{4.26}$$

where $\mathbf{f}$ presents the specific external forces and $\mathbf{\Pi}$ is the stress tensor, which is given by the equation

$$\mathbf{\Pi} = \begin{bmatrix} \sigma_1 & \tau_{12} & \tau_{13} \\ \tau_{21} & \sigma_2 & \tau_{23} \\ \tau_{31} & \tau_{32} & \sigma_3 \end{bmatrix},$$

where σ_i are normal stresses and τ_{ij} are shear stresses. Shear stresses satisfy symmetry i.e. $\tau_{ij} = \tau_{ji}$. Thus the stress tensor $\mathbf{\Pi}$ is symmetric.

External forces usually include gravitational forces. Moreover we need to attain a closed form for stress tensor $\mathbf{\Pi}$. This is done by defining a *newtonian fluid*.

Definition 4.1. Fluid is called newtonian if

$$\tau_{ij} = \mu \left(\frac{\partial u_i}{\partial x_j} + \frac{\partial u_j}{\partial x_i} \right), \tag{4.27}$$

where τ_{ij} is shear stress in i-j plane, $i \neq j$ and μ is called *viscosity*.

Most continuum gases and liquids are newtonian fluids, but not all. For instance some rubber compounds are not newtonian. In this work it is assumed that fluids are newtonian.

Normal stresses are caused by fluid flow in the normal direction and the pressure forces. We assume that normal stresses satisfy

$$\sigma_i = -p + \mu^{'} \frac{\partial u_k}{\partial x_k}, \tag{4.28}$$

where $\mu^{'}$ is called the *second viscosity*. Einstein's tensor syntax used here is defined by

$$\frac{\partial u_k}{\partial x_k} = \sum_{k'=1}^{3} \frac{\partial u_{k'}}{\partial x_{k'}}. \tag{4.29}$$

Now the stress tensor $\mathbf{\Pi}$ can be given as

$$\Pi_{ij} = \left(-p + \mu^{'} \frac{\partial u_k}{\partial x_k}\right) \delta_{ij} + \mu \left(\frac{\partial u_i}{\partial x_j} + \frac{\partial u_j}{\partial x_i}\right), \tag{4.30}$$

where δ_{ij} is the Kronecker delta function given by

$$\delta_{ij} = \begin{cases} 1 & \text{if } i = j \\ 0 & \text{if } i \neq j \end{cases}$$

Two viscosities are connected by the *bulk viscosity* given by

$$\kappa = \frac{2}{3}\mu + \mu^{'}. \tag{4.31}$$

The bulk viscosity is usually neglected except in the cases of shock wave stucture study and accoustics. Hence it will assumed that $\kappa = 0$ which yields $\mu^{'} = -\frac{2}{3}\mu$ [2].

It is common to separate stress tensor into two parts consisting of viscous terms and pressure terms. We split $\mathbf{\Pi}$ into

$$\mathbf{\Pi} = -p\mathrm{I} + \mathbb{T}, \tag{4.32}$$

where $\mathbb{T}$ is called *viscous stress tensor*. For the sake of simplicity it will be writen that, $u_1 = u$, $u_2 = v$ and $u_3 = w$. Moreover a standard 3-D space axis name convention given by $x_1 = x$, $x_2 = y$ and $x_3 = z$ will be used.

Substituting the stress tensor $\mathbf{\Pi}$ given by equation (4.30) to the general momentum conservation equation (4.26) we obtain the famous Navier-Stokes equations given by

$$
\begin{aligned}
\rho\frac{Du}{Dt} &= \rho f_x - \frac{\partial p}{\partial x} + \frac{\partial}{\partial x}\left(\frac{2}{3}\mu\left(2\frac{\partial u}{\partial x} - \frac{\partial v}{\partial y} - \frac{\partial w}{\partial z}\right)\right) \\
&\quad + \frac{\partial}{\partial y}\left(\mu\left(\frac{\partial u}{\partial y} + \frac{\partial v}{\partial x}\right)\right) + \frac{\partial}{\partial z}\left(\mu\left(\frac{\partial w}{\partial x} + \frac{\partial u}{\partial z}\right)\right) \\
\rho\frac{Dv}{Dt} &= \rho f_y - \frac{\partial p}{\partial y} + \frac{\partial}{\partial y}\left(\frac{2}{3}\mu\left(2\frac{\partial v}{\partial y} - \frac{\partial u}{\partial x} - \frac{\partial w}{\partial z}\right)\right) \\
&\quad + \frac{\partial}{\partial x}\left(\mu\left(\frac{\partial u}{\partial y} + \frac{\partial v}{\partial x}\right)\right) + \frac{\partial}{\partial z}\left(\mu\left(\frac{\partial w}{\partial y} + \frac{\partial v}{\partial z}\right)\right) \\
\rho\frac{Dw}{Dt} &= \rho f_z - \frac{\partial p}{\partial z} + \frac{\partial}{\partial z}\left(\frac{2}{3}\mu\left(2\frac{\partial w}{\partial z} - \frac{\partial u}{\partial x} - \frac{\partial v}{\partial y}\right)\right) \\
&\quad + \frac{\partial}{\partial x}\left(\mu\left(\frac{\partial u}{\partial z} + \frac{\partial w}{\partial x}\right)\right) + \frac{\partial}{\partial y}\left(\mu\left(\frac{\partial v}{\partial z} + \frac{\partial w}{\partial y}\right)\right).
\end{aligned}
$$

Using the viscous stress tensor these equations can be writen as

$$\rho\frac{D\mathbf{u}}{Dt} = \rho\mathbf{f} - \nabla p + \nabla\cdot\mathbb{T}. \tag{4.33}$$

Viscosity μ is generally a function of temperature. Thus it varies through space if there are temperature differences. We assume that the viscosity of a gas obeys the so called Sutherland's formula given by

$$\mu = \mu_0\frac{T_0 + C_S}{T + C_S}\left(\frac{T}{T_0}\right)^{3/2}, \tag{4.34}$$

where T_0 and μ_0 are reference values and C_S is Sutherland's constant for the gas [2, 13].

4.2.3 Conservation of energy

A differential form of the first law of thermodynamics can be writen as

$$\frac{\partial E_t}{\partial t} + \nabla\cdot E_t\mathbf{u} = \frac{\partial Q}{\partial t} - \nabla\cdot\mathbf{q} + \rho\mathbf{f}\cdot\mathbf{u} + \nabla\cdot(\mathbf{\Pi}\cdot\mathbf{u}), \tag{4.35}$$

where E_t is (specific) total energy, $\mathbf{q}$ is heat flux i.e. heat flow and $\frac{\partial Q}{\partial t}$ is heat generation. Heat generation can be caused for instance by nuclear or chemical reactions. The heat flux $\mathbf{q}$ is given by the Fourier's first law

$$\mathbf{q} = -k\nabla T, \tag{4.36}$$

where k is the coefficient of heat conductivity.

In this work we assume that the only significant forms of energy are internal energy and kinetic energy. This yields

$$E_t = \rho(e + \frac{1}{2}\|\mathbf{u}\|^2), \tag{4.37}$$

where e denotes internal energy instead of u to avoid confusion with velocity.

Now equation (4.35) can be formulated as

$$\rho\frac{De}{Dt} + p(\nabla \cdot \mathbf{u}) = \frac{\partial Q}{\partial t} - \nabla \cdot \mathbf{q} + \nabla \cdot (\mathbb{T} \cdot \mathbf{u}) - (\nabla \cdot \mathbb{T}) \cdot \mathbf{u}. \tag{4.38}$$

The two last terms are called the dissipation function that is given by

$$\Psi = \nabla \cdot (\mathbb{T} \cdot \mathbf{u}) - (\nabla \cdot \mathbb{T}) \cdot \mathbf{u}. \tag{4.39}$$

The dissipation function represents the rate at which the mechanical energy of the flow is turned to heat. Recall in the definition of enthalpy $h = u + p\nu$ we may write equation (4.38) as

$$\rho\frac{Dh}{Dt} = \frac{Dp}{dt} + \frac{\partial Q}{\partial t} + \nabla \cdot (k\nabla T) + \Psi. \tag{4.40}$$

It common to refer to the conservation equations (4.24), (4.33) and (4.40) as Navier-Stokes equations [2, 13].

4.3 Turbulent flow

4.3.1 General charecteristics

Recall the definition of Reynolds number

$$Re = \frac{\rho\|\mathbf{u}\|_{\text{mean}}L}{\mu}, \tag{4.41}$$

Figure 4.1: Picture showing turbulent vortex created by airplane's wing. Picture was taken from website http://www.einztein.com/tag/Aerodynamics/.

where $\|\mathbf{u}\|_{\text{mean}}$ is the mean norm of velocity and L is the characteristic length of problem for instance 1m for cars. The Reynolds number is a dimensionless number that can be used to determine wheather flow is laminar or turbulent. High Reynolds number ($Re > 5000$) indicate that the flow is turbulent.

A turbulent flow can be characterized by periodic oscillations of pressure and velocity in time and space, called eddies. Eddies may be present even when external factors are steady. Moreover the lengths of these eddies typically range from 10cm to 1cm and frequencies can be as high as 10 kHz. Thus direct solutions of Navier-Stokes equations would require very fine space and time meshing which makes them impractical or impossible for most turbulent flows.

There are semi direct solution methods based on Navier-Stokes equations which try to model only the larger eddies, namely Large Eddy Simulation (LES), but they are computationally very expensive [2, 13].

4.3.2 Reynolds equations

The idea of the Reynolds equations is to model mean flow and leave out any unnecessary information about eddies. This is done by defining the time-average of a function by

$$\bar{f} = \frac{1}{\Delta T}\int_t^{t+\Delta T} f dt^{'}. \tag{4.42}$$

The length of the time window ΔT should be large enough to cover the lowest frequency eddy. Now functions can be split in two parts, namely time-avaraged part and periodic part as

$$f = \bar{f} + f^{'}, \tag{4.43}$$

where $f^{'}$ is periodic part satisfying $\bar{f}^{'} = 0$.

The Reynolds averaged Navier-Stokes (RANS) equations are obtained from the Navier-Stokes equations (4.24), (4.33) and (4.40) by substituting equation (4.43) and invoking the time-averaging process for both sides of the equations. Before doing an actual time-avaraging there are some things that should be pointed out. We will use $\Omega \subset \mathbb{R}^n$ as the domain of the PDE.

Lemma 4.2. *Let $f \in W^{k,p}(\Omega)$, then*

$$\bar{\bar{f}} = \bar{f} \text{ and}$$

$$\overline{f^{'}\bar{f}} = 0.$$

Proof. The first equation is obtained easily by

$$\begin{aligned} \bar{\bar{f}} &= \frac{1}{\Delta t}\int_t^{t+\Delta t} \bar{f}(x,t)dt^{'} \\ &= \bar{f}\frac{1}{\Delta t}\int_t^{t+\Delta t} dt^{'} = \bar{f}. \end{aligned}$$

The second equation is obtained by

$$\begin{aligned}\overline{f'\bar{f}} &= \frac{1}{\Delta t}\int_t^{t+\Delta t} f'\bar{f}(x,t)dt' \\ &= \bar{f}\bar{f}' = \bar{f}\cdot 0 = 0.\end{aligned}$$

□

However in general $\overline{f'g'} \neq 0$. Recall the conservation of mass equation (4.24)

$$\frac{D(\bar{\rho}+\rho')}{Dt} + \rho\nabla\cdot\left(\bar{\mathbf{u}}+\mathbf{u}'\right) = 0.$$

Assuming that fluctuations of viscosity and thermal conductivity are negligible taking time-averages on both sides yields

$$\frac{\partial\bar{\rho}}{\partial t} + \frac{\partial\bar{\rho'}}{\partial t} + \nabla\cdot\left(\overline{\bar{\rho}\bar{\mathbf{u}}} + \overline{\rho'\bar{\mathbf{u}}} + \overline{\bar{\rho}\mathbf{u}'} + \overline{\rho'\mathbf{u}'}\right) = 0. \tag{4.44}$$

Invoking lemma 4.2 on equation (4.44) gives

$$\frac{\partial\bar{\rho}}{\partial t} + \nabla\cdot\left(\bar{\rho}\bar{\mathbf{u}} + \overline{\rho'\mathbf{u}'}\right) = 0. \tag{4.45}$$

In general only mixed fluctuating terms like $\overline{\rho'\mathbf{u}'}$ remain in the RANS equations. Invoking similar time-averaging on the conservation of momentum equations (4.33) and the conservation of energy equation (4.40) yields

$$\frac{\partial}{\partial t}\left(\bar{\rho}\bar{\mathbf{u}} + \overline{\rho'\mathbf{u}'}\right) + \nabla\cdot\left(\bar{\rho}\bar{\mathbf{u}}\bar{\mathbf{u}} + \bar{\mathbf{u}}\overline{\rho'\mathbf{u}'}\right) = -\nabla\bar{p} + \nabla\cdot\left(\bar{\mathbb{T}} - \bar{\mathbf{u}}\overline{\rho'\mathbf{u}'} - \bar{\rho}\overline{\mathbf{u}'\mathbf{u}'} - \overline{\rho'\mathbf{u}'\mathbf{u}'}\right) \tag{4.46}$$

and

$$\rho\frac{\partial\bar{h}}{\partial t} + \overline{\rho'\frac{\partial h'}{\partial t}} + \bar{\rho}\bar{\mathbf{u}}\cdot\nabla\bar{h} + \bar{\rho}\overline{\mathbf{u}'\cdot\nabla h'} + \overline{\rho'\bar{\mathbf{u}}\cdot\nabla h'} + \overline{\rho'\mathbf{u}'\cdot\nabla\bar{h}} + \tag{4.47}$$

$$\overline{\rho'\mathbf{u}'\nabla p'} = \frac{\partial\bar{p}}{\partial t} + \bar{\mathbf{u}}\cdot\nabla\bar{h} + \overline{\mathbf{u}'\cdot\nabla p'} + \nabla\cdot\left(k\nabla\bar{T}\right) + \overline{\frac{\partial Q}{\partial t}} + \overline{\Psi}. \tag{4.48}$$

Here the time-averaged viscous stress tensor $\bar{\mathbb{T}}$ is given by

$$\bar{\mathbb{T}}_{ij} = \mu\left(\left(\frac{\partial \bar{u}_i}{\partial x_j} + \frac{\partial \bar{u}_j}{\partial x_i}\right) - \frac{2}{3}\delta_{ij}\frac{\partial \bar{u}_k}{\partial x_k}\right). \tag{4.49}$$

Moreover the time-averaged dissipation function $\overline{\Psi}$ is given by

$$\Psi = \nabla \cdot \left(\overline{\mathbb{T}}\overline{\mathbf{u}} + \overline{\mathbb{T}'\mathbf{u}'}\right) - (\nabla \cdot \overline{\mathbb{T}}) \cdot \bar{\mathbf{u}} - \overline{(\nabla \cdot \mathbb{T}') \cdot \mathbf{u}'}. \tag{4.50}$$

The fluctuating viscous stress tensor is given by an equation similar to equation (4.49)

$$\mathbb{T}'_{ij} = \mu\left(\left(\frac{\partial u_i'}{\partial x_j} + \frac{\partial u_j'}{\partial x_i}\right) - \frac{2}{3}\delta_{ij}\frac{\partial u_k'}{\partial x_k}\right). \tag{4.51}$$

It should be clear that RANS equations are far more complex than original Navier-Stokes equations. Moreover they introduce new unknown functions (21 new functions from fluctuating time-averaged cross terms), which makes computation more expensive. However RANS equations allow a sparser mesh to be used than the Navier-Stokes equations and therefore ease the computational load. In practice the advantage of sparser mesh outweight the disadvantage of the new unknown functions. Another disadvantage in introducing new unknown functions is that they make the underlying equation system (RANS equations) underdetermined. Therefore in order to solve these equations new equations must be added.

These additional equations are usually called turbulence models. In this thesis we will use so called k-ε turbulence model explained in section 4.3.3. In general turbulence models can be split into two categories, those that rely on the Boussinesq assumption and those that do not. Methods relying on the Boussinesq assumption are called *turbulent viscosity models*. Usually turbulent viscosity models are computationally less expensive. Another class of methods that don't rely on Boussinesq assumption are usually called *Reynold's stress models*. These models are computationally more expensive and usually position themselves between turbulent viscosity models and LES [2, 13, 1].

4.3.3 k-ε turbulence model

The k-ε turbulence model is based on the Boussinesq assumption mentioned before. The Boussinesq assumption is given by

$$\bar{\rho}\overline{u_i' u_j'} = \mu_T\left(\frac{\partial \bar{u}_i}{\partial x_j} + \frac{\partial \bar{u}_j}{\partial x_i}\right) - \frac{2}{3}\delta_{ij}\left(\mu_T\frac{\partial \bar{u}_k}{\partial x_k} + \bar{\rho}k'\right), \tag{4.52}$$

where $\bar{k}$ is the kinetic energy of turbulence and μ_T is the *turbulent viscosity*. The kinetic of energy of turbulence is given by

$$k^{'} = \frac{\overline{u_k^{'} u_k^{'}}}{2}. \tag{4.53}$$

Boussinesq assumption states that turbulent shearing stresses are connected to time-averaged velocity gradients by turbulent viscosity. The k-ε model is one way to model the turbulent viscosity μ_T. Kolmogorov-Prandtl equation states that the turbulent kinetic energy and the turbulent viscosity are connected by

$$\mu_T = C_1 \bar{\rho} \sqrt{k'} L^*, \tag{4.54}$$

where C_1 is a constant and L^* is the characteristic length of turbulent eddies, called the *turbulent length scale*.

The dissipation rate of kinetic energy is given by

$$\varepsilon = \overline{\varepsilon} + \varepsilon^{'} = 2\mu \mathbf{D} \cdot \mathbf{D}. \tag{4.55}$$

The k-ε model consists of two equations governing kinetic energy conservation and the dissipation rate of kinetic energy given by

$$\begin{aligned} &\frac{1}{\sqrt{g}} \frac{\partial}{\partial t} \left(\sqrt{g} \bar{\rho} k^{'} \right) + \frac{\partial}{\partial x_j} \left(\rho \overline{u}_j k^{'} - \left(\mu + \frac{\mu_T}{\sigma_k} \right) \frac{\partial k^{'}}{\partial x_j} \right) = \\ &\mu_T \left(P + P_B \right) - \overline{\rho} \varepsilon^{'} - \frac{2}{3} \left(\mu_T \frac{\partial \overline{u}_i}{\partial x_i} + \overline{\rho} k^{'} \right) \frac{\partial \overline{u}_i}{\partial x_i} + \mu_T P_{NL} \end{aligned} \tag{4.56}$$

and

$$\begin{aligned} &\frac{1}{\sqrt{g}} \frac{\partial}{\partial t} \left(\sqrt{g} \bar{\rho} \varepsilon^{'} \right) + \frac{\partial}{\partial x_j} \left(\overline{\rho u}_j \varepsilon^{'} - \left(\mu + \frac{\mu_T}{\sigma_\varepsilon} \right) \frac{\partial \varepsilon^{'}}{\partial x_j} \right) = \\ &C_{\varepsilon 1} \frac{\varepsilon^{'}}{k^{'}} \left(\mu_T P - \frac{2}{3} \left(\mu_T \frac{\partial \overline{u}_i}{\partial x_i} + \overline{\rho} k^{'} \right) \frac{\partial \overline{u}_i}{\partial x_i} \right) + \\ &C_{\varepsilon 3} \frac{\varepsilon^{'}}{k^{'}} \mu_T P_B - C_{\varepsilon 2} \overline{\rho} \frac{\varepsilon^{'2}}{k^{'}} + C_{\varepsilon 4} \overline{\rho} \varepsilon^{'} \frac{\partial \overline{u}_i}{\partial x_i} + C_{\varepsilon 1} \frac{\varepsilon^{'}}{k^{'}} \mu_T P_{NL}, \end{aligned} \tag{4.57}$$

where

$$P = \overline{\rho}\overline{u_i^{'}u_j^{'}}\frac{\partial \overline{u}_j}{\partial x_i}, \tag{4.58}$$

$$P_B = -\beta g_i \frac{\mu_T}{Pr_t}\frac{\partial T}{\partial t}, \tag{4.59}$$

where g_i is i:th gravitational component, $Pr_T = 0.85$ is the Prandtl number and β the coefficient of thermal expansion given by

$$\beta = -\rho^{-1}\left(\frac{\partial \rho}{\partial T}\right)_p, \tag{4.60}$$

where the subscript p denote that derivation is done assuming constant pressure and

$$P_{NL} = -\frac{P}{\mu_T} - \left(P - \frac{2}{3}\left(\frac{\partial \overline{u}_i}{\partial x_i} + \frac{\overline{\rho}k^{'}}{\mu_T}\right)\frac{\partial \overline{u}_i}{\partial x_i}\right). \tag{4.61}$$

Moreover k-ε model connects turbulent viscosity to $k^{'}$ and $\varepsilon^{'}$ by

$$\mu_T = f_\mu \frac{C_\mu \overline{\rho} k'^2}{\varepsilon^{'}}. \tag{4.62}$$

The values of the coefficients are described in the following Table 4.3.3 [13, 1].

Name	Value
C_μ	0.09
σ_k	1.0
σ_ε	1.22
σ_h	0.9
σ_m	0.9
$C_{\varepsilon 1}$	1.44
$C_{\varepsilon 2}$	1.92
$C_{\varepsilon 3}$	0.0 or 1.44 [1]
$C_{\varepsilon 4}$	−0.33

In addition it is customary to use a wall model close to a solid boundary. This is due to fast property changes near solid boundaries. In this work we will present the All y+ wall treatment, which is usually used in high Reynolds number flows.

[1] If $P_B > 0$ then 1.44 and zero otherwise

We begin by introducing new dimensionless properties, namely u^+ and y^+, which are given by equations

$$u^+ = \frac{u - u_w}{\sqrt{\tau_w/\rho}} \tag{4.63}$$

and

$$y^+ = \frac{y\sqrt{\tau_w/\rho}}{\nu}, \tag{4.64}$$

where u is the tangential velocity, u_w the wall velocity, τ_w the shear stress at the wall, ν the dynamic viscosity given by μ/ρ and y the distance from the wall. Assuming a newtonian fluid and that shear stress remains almost constant near the wall, we may write the shear stress at the wall as

$$\tau_w = \mu\frac{\partial u}{\partial y}. \tag{4.65}$$

Combining equations (4.63)-(4.65), assuming that $u_w = 0$ and thus tangential velocity vanishes at the wall we obtain

$$u^+ = y^+. \tag{4.66}$$

In light of measurements equation (4.66) is accurate when $y^+ < 5$ [12]. Farther away from the wall turbulent stresses grow larger and equation (4.66) is no longer feasible. Assuming that viscosity is negligible compared to turbulent viscosity we may write

$$\tau_w = \rho\kappa u_\tau y\frac{\partial u}{\partial y}, \tag{4.67}$$

where $u_\tau = \sqrt{\tau_w/\rho}$. Substituting equations (4.67) to equations (4.63) and (4.64) we obtain

$$u^+ = \frac{1}{\kappa}\ln\left(y^+\right) + C, \tag{4.68}$$

where κ is a constant, usually set to 0.4 and C is also a constant, which is usually taken to be 5.5. Measurements imply that the equation (4.68) is applicable when $y^+ > 30$

[12]. There are also models for $5 < y^+ < 30$, such as the Van Driest turbulence model, which are not discussed in this thesis.

4.4 Nozzle flow

4.4.1 Basic properties

In this section we will discuss the general features of nozzle flow. We derive some principal features of nozzle flows from simplified Navier-Stokes equations. Simplified Navier-Stokes equations are used because explicit formulae for nozzle flow can be obtained. If we ignore friction i.e. set viscosity $\mu = 0$ in equation (4.33) we obtain the Euler equations which govern inviscid flow. The Euler equations are given by

$$\rho \frac{D\mathbf{u}}{Dt} = \rho \mathbf{f} - \nabla p. \tag{4.69}$$

A nozzle is a device that is used to accelerate fluid flow without external power input as opposed to for instance a pump. Nozzles are usually pipes whose cross section varies. Pressure at the inlet of a nozzle is called inlet pressure and pressure at the outlet is called back pressure. The most narrow section of the nozzle is called the throat.

Since fluid flow in the normal direction of a pipe is usually small compared to the principal direction we assume that velocities in the normal directions are negligible. We also omit external forces such as gravitation. Thus only the Euler equation governing flow in the principal direction is meaningful. Moreover assuming that flow is steady i.e $\frac{\partial}{\partial t} = 0$ and that principal flow is symmetric at cross section we obtain

$$\rho u \left(\frac{\partial u}{\partial x} + \frac{\partial u}{\partial y} \right) = - \left(\frac{\partial p}{\partial x} + \frac{\partial p}{\partial y} \right). \tag{4.70}$$

Assuming constant flow over a cross section i.e $\frac{\partial}{\partial y} = 0$ equation (4.70) yields in differential form

$$u du + \frac{dp}{\rho} = 0, \tag{4.71}$$

which is the famous Bernoulli equation for compressible flow. The Bernoulli equation is commonly used to calculate pressure from a velocity field even through it is only valid for inviscid flow.

Moreover conservation of mass can be written in integral form as

$$\int_{A(x_1)} \rho u dy = \int_{A(x_2)} \rho u dy. \tag{4.72}$$

Assuming constant flow over a cross section i.e $\frac{\partial}{\partial y} = 0$ yields

$$A_1 \rho_1 u_1 = A_2 \rho_2 u_2, \tag{4.73}$$

where subscripts one and two refer to different cross sections. Thus

$$\frac{u_1}{u_2} \propto \frac{A_2}{A_1}. \tag{4.74}$$

In light of the equation (4.74) it follows that a converging nozzle will accelerate the flow. This is true for subsonic flows. However for supersonic flows a converging nozzle decelerate the flow.

Let c be the speed of a sound wave in fluid. Recall that the speed of sound in a fluid is given by

$$c^2 = \frac{\partial p}{\partial \rho}. \tag{4.75}$$

Conservation of mass for nozzle flows with constant velocity over a cross section can be writen as

$$d(\rho u A) = 0. \tag{4.76}$$

Dividing equation (4.76) by $\rho u A$ and denoting $M = u/c$ yields

$$\begin{aligned} \frac{d\rho}{\rho} + \frac{du}{u} + \frac{dA}{A} &= \frac{1}{c^2}\left(c^2 \frac{d\rho}{\rho}\right) + \frac{dM}{M} + \frac{dA}{A} \\ &= \frac{1}{c^2}\frac{\partial p}{\rho} + \frac{dM}{M} + \frac{dA}{A} \\ &= -M dM + \frac{dM}{M} + \frac{dA}{A} = 0. \end{aligned}$$

Thus we may write

$$\left(M - \frac{1}{M}\right) dM = \frac{dA}{A}. \tag{4.77}$$

If a flow is subsonic ($M < 1$) decreasing cross section ($dA < 0$) accelerates flow. However if it is supersonic ($M > 1$) decreasing cross section $dA < 0$ decelerates flow. Hence in order to accelerate fluid flow to supersonic level a single divergencing nozzle is not enough and flow velocity will be stuck at transonic speed ($M = 1$).

In order to accelerate compressible flow to supersonic speeds one must employ a diverging-converging nozzle called Laval nozzle or DC-nozzle. In a Laval nozzle it is crucial that the flow speed be at transonic level when it enters the throat. Otherwise the converging section of nozzle will start to slow it down as equation (4.77) predicts. Fluid could pass through throat at a supersonic speed, but experience a shock wave which slows it down to the subsonic level. Shock waves can be observed as a sudden rise of a pressure. Shock waves are usually modelled as discontinuities in solution due to very narrow time frame of whole event. They also result in a loss of stagnation pressure, therefore transforming pressure and kinetic energy of the gas to heat. Shock waves can be split to oblique shock waves proceeding in the principal flow direction and normal shock waves taking place in normal directions. A more detail discussion of shock waves and nozzle design will be presented in section 4.4.2.

Figure 4.2: Picture showing Mack shock discs in jet stream of afterburning turbojet engine. Picture is taken from website http://en.wikipedia.org/wiki/Shock_diamond.

Another major factor in nozzle is back pressure. If the back pressure of gas leaving the nozzle is less than (greater than) the ambient pressure, nozzle jet is called overexpanded (underexpanded). Incorrect expansion of a jet will cause Mach shock discs in the jet stream. Figure 4.2 shows an example of a Mach shock discs.

The physical explenation of Mach shock discs is that incorrect expansion will create normal flow velocities due to existence of a normal pressure gradient. These normal flows give rise to periodic compression of the jet stream which appears as Mach shock discs. As the pressure of a Mach shock disc is larger than its surroundings it will cause gas to flow out of the Mach shock disc and create a low pressure area beneath it due to the inertia of the gas which then repeats the shock disc. Creation of Mach shock discs are explained in Figures 4.3 and 4.4.

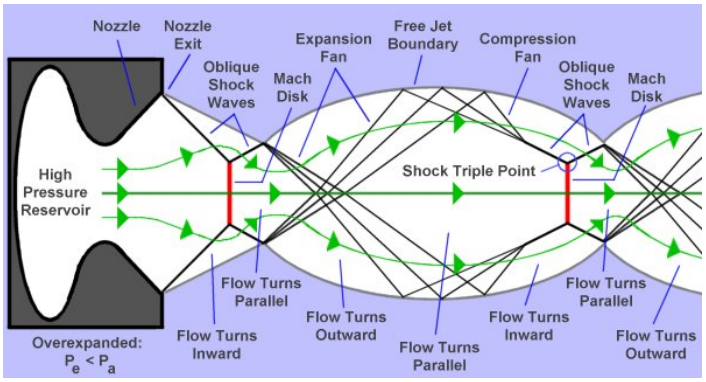

Figure 4.3: Illustration of the birth of mach shock discs due to over expansion. Picture is taken from website http://www.aerospaceweb.org/question/propulsion/q0224.shtml.

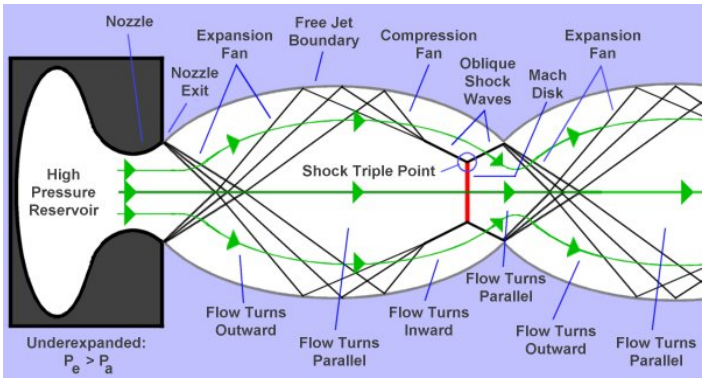

Figure 4.4: Illustration of the birth of mach shock discs due to under expansion. Picture is taken from website http://www.aerospaceweb.org/question/propulsion/q0224.shtml.

The equations and some assumptions presented here are not applicable to actual simulation of flow. They were merely presented to show some fundamental properties of the nozzle flow. In particular the velocity profile in a cross section of a nozzle is never constant [21].

4.4.2 Wave propogation in fluids.

We begin our discussion with sound waves. Sound waves are propagating pressure oscillations in a medium. Since a single oscillation of sound waves takes place in a very narrow time window it is customary to assume that it is isentropic $dS = 0$.

For isentropic ideal gas processes we have

$$d\left(pV^{\gamma}\right) = 0. \tag{4.78}$$

By differentiating equation (4.78) we obtain

$$\frac{dp}{d\rho} = \gamma\frac{p}{\rho} = \gamma R_M T = c^2. \tag{4.79}$$

We proceed by introducing the linearized Navier-Stokes equations. The linearized conservation of mass equation is given by

$$\frac{\partial\rho}{\partial t} + \rho_0\nabla\cdot\mathbf{u} = 0, \tag{4.80}$$

where ρ_0 is a typical value for density and taken to be constant. The linearized conservation of momentum equation is given by

$$\rho_0\left(\frac{\partial\mathbf{u}}{\partial t} + \mathbf{u}\cdot\nabla\mathbf{u}\right) = -\nabla p + \nabla\cdot\mathbb{T}. \tag{4.81}$$

Linearization of Navier-Stokes equations can be justified if changes in density are small relative to other variables. Differentiating equation (4.80) with respect to time gives

$$\frac{\partial^2\rho}{\partial t^2} = -\rho_0\nabla\cdot\left(\frac{\partial\mathbf{u}}{\partial t}\right). \tag{4.82}$$

Taking the divergence on both sides of equation (4.81) we obtain

$$\rho_0\nabla\cdot\left(\frac{\partial\mathbf{u}}{\partial t}\right) = -\nabla^2 p - \rho_0\nabla\cdot(\mathbf{u}\cdot\nabla\mathbf{u}) + \nabla\cdot\nabla\cdot\mathbb{T}. \tag{4.83}$$

Combining equations (4.82) and (4.83) we obtain

$$\nabla^2 p = \frac{\partial^2 \rho}{\partial t^2} - \rho_0 \nabla \cdot (\mathbf{u} \cdot \nabla \mathbf{u}) + \nabla \cdot \nabla \cdot \mathbb{T}. \tag{4.84}$$

Assuming inviscid flow ($\mu = 0$) we obtain

$$\nabla^2 p = \frac{\partial^2 \rho}{\partial t^2} - \rho_0 \nabla \cdot (\mathbf{u} \cdot \nabla \mathbf{u}) \,. \tag{4.85}$$

Since sound waves cause only a minor disturbance to speed in comparison to pressure we have $\mathbf{u} \cdot \nabla \mathbf{u} \ll \nabla p$. Hence we may drop last term from equation (4.85) and obtain

$$c^2 \nabla^2 p = \frac{\partial^2 p}{\partial t^2}, \tag{4.86}$$

which justifies our use of c as a speed of sound [7].

Pressure disturbations give rise to sound waves. Suppose a object launched at the origin and moving with speed of $\mathbf{u}$ in the direction of the positive x-axis and transmitting sound waves. This is usually modelled by adding a source term on the right hand side of wave equation

$$c^2 \nabla^2 p - \frac{\partial^2 p}{\partial t^2} = s(t)\delta^3(\mathbf{x} - \mathbf{u}t), \tag{4.87}$$

where $s(t)$ is a source function and δ^3 is Dirac's delta function having the property of

$$\int_{\mathbb{R}^n} \delta^n d\mathbf{x} = 1, \tag{4.88}$$

and

$$\delta^3(\mathbf{x}) = \begin{cases} \infty & \text{if } \mathbf{x} = 0 \\ 0 & \text{otherwise} \end{cases}$$

Moreover we set boundary constraints as

$$p(\mathbf{x}, t) = 0, \text{ for all } \mathbf{x}, \tag{4.89}$$

$$\frac{\partial p(\mathbf{x}, 0)}{\partial t} = \begin{cases} \frac{ds(0)}{dt} & \text{if } \mathbf{x} = 0 \\ 0 & \text{otherwise} \end{cases}$$

Solution to the single disturbance $\delta^3(\mathbf{x}-\eta)$ is given by

$$p_\eta(\mathbf{x},t) = \begin{cases} H\left((ct)^2 - \|\mathbf{x}-\eta\|^2\right) & \text{if } t \geq 0 \\ 0 & \text{otherwise} \end{cases}$$

Here H is called the Heaviside function and is given by

$$H(x) = \int_{-\infty}^{x} \delta(x)dx. \tag{4.90}$$

The general solution to problem (4.87) is acquired by taking a linear combination of these solutions and shifting time and place to match the source term. For simplicity we set $s(t) = 1$. The general solution is given by

$$p(\mathbf{x},t) = \int_0^t p_{\mathbf{u}t'}(\mathbf{x}-\mathbf{u}t, t-t')dt'. \tag{4.91}$$

Our interest lies in finding the boundary of the pressure wave. In case of $u = 0$ this boundary is a circle centered at the wave source. As speed increases the boundary of wave starts to bend and at transonic speed $u = c$ forms a sharp edge at wave source.

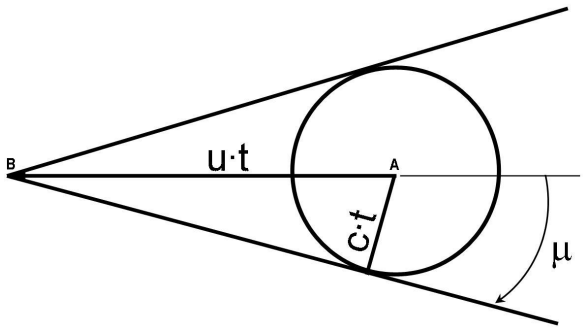

Figure 4.5: A figure showing formation of wave front from spherical shock waves.

Since each wavefront (solutions of equation (4.4.2)) is circle centered at $\mathbf{u}t$ with radius of ct, boundaries of these circles must lie between two lines at a given moment. If $u \geq c$ these lines must intersect at the wavesources' present location. Each point of the wave front (the line) is part of the unique circular wave (4.4.2). These lines are called the Mach lines or the Mach waves. The angle between x-axis and the Mach wave is called the Mach angle and is given by

$$\sin(\mu_M) = M^{-1}, \tag{4.92}$$

where M^{-1} is the Mach number of the wave source. The same phenomenon takes place if the wave source is at a standstill and the fluid is moving at supersonic speed relative to the wave source [21].

4.4.3 Prandtl-Meyer expansion fans

In this section we discuss the concept of Prandtl-Meyer flow. We also explain why a smoothly expanded flow is isentropic and derive the connection between velocity and turn of flow. We begin our discussion with normal shock waves and the changes that they cause in pressure, velocity and entropy.

Normal shock waves may cause sudden rises in pressure. However this pressure rise has to conserve energy and mass. Moreover stagnation temperature has to remain constant during a shock wave. This is because there are no external addition of heat or work in a shock wave. Let subscript 1 denote the properties before the shock wave and 2 after the shock wave. Due to the constant stagnation temperature we have

$$T_1\left(1+\frac{\gamma-1}{2}M_1^2\right)=T_2\left(1+\frac{\gamma-1}{2}M_2^2\right), \tag{4.93}$$

where M_1 and M_2 are Mach numbers. It should be noted that since the shock wave under discussion is a normal shock wave, velocities are normal to the shock wave front.

The ideal gas law (4.1) yields

$$\begin{aligned}\frac{T_2}{T_1} &= \frac{p_2\rho_1}{p_1\rho_2}=\frac{p_2u_2}{p_1u_1}=\frac{p_2}{p_1}\frac{c_2}{c_1}\frac{M_2}{M_1}\\ &= \frac{p_2}{p_1}\left(\frac{T_2}{T_1}\right)^{1/2}\frac{M_2}{M_1}=\frac{p_2}{p_1}\left(\frac{1+\frac{\gamma-1}{2}M_1^2}{1+\frac{\gamma-1}{2}M_2^2}\right)^{1/2}\frac{M_2}{M_1}.\end{aligned}$$

Thus the pressure ratio between before and after the normal shock wave is given as

$$\frac{p_2}{p_1}=\left(\frac{1+\frac{\gamma-1}{2}M_1^2}{1+\frac{\gamma-1}{2}M_2^2}\right)^{1/2}\frac{M_2}{M_1}. \tag{4.94}$$

Omitting external forces like gravitation, conservation of momentum yields

$$p_1+\rho_1u_1^2=p_2+\rho_2u_2^2. \tag{4.95}$$

Solving for pressure ratio from equation (4.95) yields

$$\frac{p_2}{p_1} = \frac{1+\gamma M_1^2}{1+\gamma M_2^2}. \tag{4.96}$$

Combining equations (4.94) and (4.96) we obtain

$$M_2^2 = \frac{(\gamma-1)\,M_1^2+2}{2\gamma M_1^2-(\gamma-1)}. \tag{4.97}$$

Thus a normal shock wave may change the Mach number of a flow only by a certain amount depending on the Mach number before the shock wave. Moreover combining equations (4.94) and (4.97) we get

$$\frac{p_2-p_1}{p_1} = \frac{2\gamma}{\gamma+1}\left(M_1^2-1\right), \tag{4.98}$$

which states that relative pressure change depends only on the Mach number before the shock wave. Also a measure of entropy change during a shock wave is needed. Entropy change of an ideal gas is given by

$$\frac{s_2-s_1}{R} = \frac{\gamma}{\gamma-1}\ln\left(\frac{\rho_1}{\rho_2}\right) + \frac{1}{\gamma-1}\ln\left(\frac{p_2}{p_1}\right), \tag{4.99}$$

where R is the universal ideal gas constant. Substituting equation (4.97) into equation (4.99) and invoking ideal gas law to the ratio of densities we obtain

$$\frac{s_2-s_1}{R} = \ln\left(\left(1+\frac{2\gamma}{\gamma+1}\left(M_1^2-1\right)\right)^{1/(\gamma-1)}\left(\frac{(\gamma+1)\,M_1^2}{(\gamma-1)\,M_1^2+2}\right)^{-\gamma/(\gamma-1)}\right). \tag{4.100}$$

For simplicity we define a new variable $m = M_1^2 - 1$. Recall that the logarithm has a Taylor series expansion given by

$$\ln(1+m) = m - \frac{m^2}{2} + \frac{m^3}{3} - \frac{m^4}{4} + \cdots. \tag{4.101}$$

Invoking this Taylor series expansion to equation (4.100) we obtain

$$\frac{s_2 - s_1}{R} = \frac{2\gamma}{3\left(\gamma+1\right)^2} m^3 + O(m^4), \tag{4.102}$$

where $O(m^4)$ is an O-function having the property that $O(m^4) \leq km^4$, when $m \to 0$ for some constant k.

Now assume a nearly transonic flow $M_1 \approx 1$ near a solid boundary which turns suddenly by an angle θ. In this arrangement the edge can be thought of as a wave source and shock waves are travelling downstream as explained in previous section. Equations (4.98) and (4.100) hold for the normal component of this Mach shock wave.

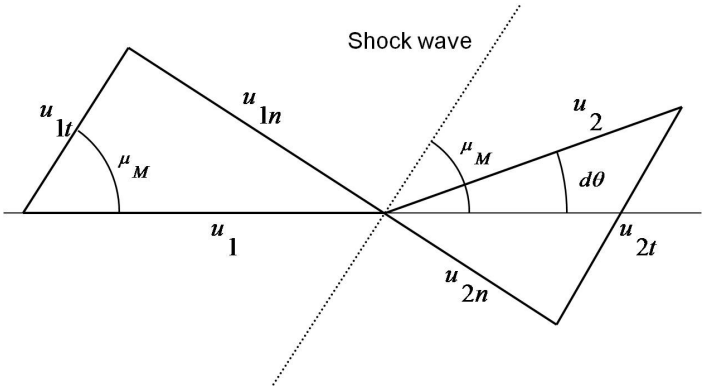

Figure 4.6: A figure demostrating conservation of the tangential velocity, when the flow is turned an angle of $d\theta$ due to a shock wave. The shock wave is shown as the dashed line.

It should be noted that the shock wave cannot change velocity tangential to the wave front. If the angle of the shock wave front is θ and flow is turned by an angle β and the Mach number of flow is M_1 before and M_2 after the shock wave front then the angles are connected by

$$\tan\theta = \frac{2\cot\beta\left(M_1^2 \sin^2(\beta) - 1\right)}{M_1^2\left(\gamma + \cos 2\beta\right) + 2}. \tag{4.103}$$

Since $M_1 \sin\beta$ is the normal component of the velocity relative to the wave front we have $m = M_1 \sin\beta$. We may write the relative pressure change as

$$\frac{p_2 - p_1}{p_1} = \frac{2\gamma}{\gamma+1}\left(M_1^2 \sin\beta - 1\right). \tag{4.104}$$

When $\theta \to 0$ we have $\beta \to \mu_M$ and $\tan\theta \to \theta$. Thus the pressure change is proportional to the angle given by

$$\Delta p \propto \frac{p_2 - p_1}{p_1} \propto \theta \tag{4.105}$$

and entropy change to third power given by

$$\Delta s \propto \frac{s_2 - s_1}{R} \propto \theta^3. \tag{4.106}$$

In case turn is made in n turns each turn being θ/n we may write total entropy change and total pressure change as sums of pressure and entropy changes of one turn. The total pressure change is given by

$$\Delta p_{\text{total}} = \sum \Delta p_{\text{single}} \propto \sum \frac{\theta}{n} = \theta. \tag{4.107}$$

However the entropy change is given by

$$\Delta s_{\text{total}} = \sum \Delta s_{\text{single}} \propto \sum \frac{\theta^3}{n^3} = \frac{\theta^3}{n^2} \to 0, \tag{4.108}$$

when $n \to \infty$. Thus a smooth turn is isentropic. Moreover since it is adiabatic it follows that it has to be also reversible and hence doesn't involve energy loss through shock waves. This kind of isentropic expansion or compression is called a Prandtl-Meyer flow.

When turning is executed smoothly and flow is isentropic the actual relationship between the angle of the entire turn and the final Mach number is of great interest. We consider an infinitesimal turn $d\theta$ and assume that it changes velocity by du. A positive angle is thought to correspond with expansion. A shock wave front generated by an infinitesimal turn must have Mach angle μ_M to the initial velocity. Like before it may not change the tangential velocity relative to the shock wave front. This conservation of tangential velocity yields in differential form

$$d\theta = \cot \mu_M \frac{du}{u} = \sqrt{M^2 - 1}\frac{du}{u}. \tag{4.109}$$

Knowing that $u = Mc$. Thus invoking $c^2 = \gamma RT$ we obtain

$$\begin{aligned} du &= d\left(Mc\right) = cdM + Md\left(\sqrt{\gamma RT}\right) \\ &= cdM + \frac{M}{2}\sqrt{\frac{\gamma R}{T}}dT. \end{aligned}$$

Combining equations we get

$$\frac{du}{u} = \frac{dM}{M} + \frac{dT}{2T}. \tag{4.110}$$

Recalling the definition of stagnation temperature and that it remains constant during the expansion we obtain

$$dT_S = dT\left(1 + \frac{\gamma - 1}{2}M^2\right) + T\left(\gamma - 1\right)MdM = 0. \tag{4.111}$$

Combining equations (4.109), (4.110) and (4.111) we get

$$d\theta = \frac{\left(M^2 - 1\right)^{1/2}}{1 + \frac{\gamma-1}{2}}\frac{dM}{M}. \tag{4.112}$$

Integrating the equation and setting that when $\theta = 0$ we have $M = M_0$, we get

$$\theta(M) = \int_{M_0}^{M} \frac{\left(M^2 - 1\right)^{1/2}}{1 + \frac{\gamma-1}{2}}\frac{dM}{M}, \tag{4.113}$$

which is called the Prandtl-Meyer function and connects the total turn angle in Prandtl-Meyer flow to final velocity [21, 14, 3, 17].

This explains how much nozzle has to be expanded to get certain Mach number, but does not describe how it should be expanded i.e. shape of nozzle wall. To answer this we have to consider reflections of shock waves.

The principal idea of designing a nozzle wall shape is to eliminate shock wave reflections. Once a shock wave front hits a wall it is reflected from it at some angle. If the angle of attack i.e. the angle of the shock wave front and the wall is suitable then wave is reflected at the same angle as wall exists and nullfied at wall. Wall should be designed in such a way that it nullfies shock waves and hence avoids interference to form a strong shock wave, which could slow velocity to subsonic mach numbers.

In general this can be done by solving the wave equation. However due to machining limitations only piecewise linear nozzle surfaces can be machined. Hence modelling is usually executed by a finite number of wave fronts. Each wavefront defines a certain piece of a nozzle.

Chapter 5

Numerical solutions of Reynolds equations

This chapters explain how RANS equations can be solved numerically. As explained before the most important details are in the evaluation of fluxes. Moreover time is handled differently from space dimensions.

5.1 Discretization

5.1.1 Fluxes in fluid dynamics

A general conservation equation can be given as

$$\frac{\partial \psi}{\partial t} + \nabla \cdot \mathbf{\Phi} = q_\psi, \tag{5.1}$$

where ψ denotes a quantity, $\mathbf{\Phi}$ is the flux of the quantity and q_ψ is the source of the quantity. Following Table 5.1 shows formulae for each symbol and each conservation equation (except the turbulence models)

Integrating equation (5.1) over domain Ω and invoking the divergence theorem we obtain

$$\frac{\partial}{\partial t}\int_\Omega \psi dV + \int_{\partial\Omega} \mathbf{\Phi} \cdot \mathbf{dS} = \int_{\mathbf{\Omega}} \mathbf{q}_\psi \mathbf{dV}. \tag{5.2}$$

Equation	ψ	Φ	q_ψ
Con. mass	ρ	$\rho\mathbf{u}$	0
Con. momentum	$\rho\mathbf{u}$	$\rho\mathbf{uu} + \mathbb{T}$	$\rho\mathbf{f}$
Cons. energy	ρe	$\rho e\mathbf{u} - \mathbf{k}\nabla\mathbf{T} + \nabla\cdot(\mathbf{pu}) + \nabla\cdot(\mathbb{T}\cdot\mathbf{u})$	$\rho\mathbf{f}\cdot\mathbf{u} + \partial\mathbf{Q}/\partial\mathbf{t}$

Table 5.1

If Ω is polyhedrons with n faces and we approximate functions and fluxes by average values at each face we obtain

$$\frac{\partial}{\partial t}(\psi V) - q_\psi V + \sum_{\partial\Omega_i} \mathbf{\Phi}\cdot\partial\mathbf{\Omega_j} = \mathbf{0}. \tag{5.3}$$

Moreover if Ω_1 and Ω_2 are two adjacent polyhedron (we will refer to such polyhedrona as cells from now on) and $\partial\Omega_C$ is the common face between two cells, fluxes Φ_{12} and Φ_{21} through the face must satisfy

$$\Phi_{12} = -\Phi_{21}. \tag{5.4}$$

Sign of the flux is assumed to be positive if it is out of the cell. The volume and face areas of the cell are obtained by vector calculus [13].

5.1.2 Flux evaluation

Since fluxes are connected to the values of variables inside the cell we need some way to evaluate them in terms of these variables. We consider a so called *cell-centered scheme*, where the values are cell specific. There is also scheme called the *cell-vertex scheme*, where the values are specified at each vertex of cell.

Now let Ω_1 and Ω_2 be adjacent cells with a common face $\partial\Omega_i$. The flux Φ in the common face may be evaluated by the cell 1 as Φ_1 or by the cell 2 as Φ_2. Thus it is natural to evaluate the flux as the avarage value given by

$$\Phi = \frac{1}{2}(\Phi_1 + \Phi_2). \tag{5.5}$$

We will discuss the magnitude of errors caused by this scheme in section 5.1.4 [13].

5.1.3 Time discretization

Space dimensions are discretized by introduction of fluxes and avarage values. Time derivatives are usually approximated through finite differences. The specific finite difference scheme should be chosen according to the steadiness of the problem. For steady problems accuracy in time is not important as it is for unsteady problems, thus a less accurate scheme can be used. In this section we introduce the finite difference schemes used in this work and show the actual discretization of the underlying equation.

Partial derivatives can be approximated by the forward difference formula given by

$$\frac{\partial \psi}{\partial t} = \frac{\psi(t + \Delta t) - \psi(t)}{\Delta t} + O(\Delta t). \tag{5.6}$$

Similarly the backward difference formula is given by

$$\frac{\partial \psi}{\partial t} = \frac{\psi(t) - \psi(t - \Delta t)}{\Delta t} + O(\Delta t). \tag{5.7}$$

Combining equations (5.6) and (5.7) we obtain central difference formula [2]

$$\frac{\partial \psi}{\partial t} = \frac{\psi(t + \Delta t) - \psi(t - \Delta t)}{2\Delta t} + O(\Delta t^2), \tag{5.8}$$

which has second order accuracy instead of first order.

Now let i, j, k denote cells space indexes and n time. For instance u^n_{ijk} is the velocity at the n:th time step in cell i, j, k. We will omit O functions for the rest of this section and discuss accuracy considerations in section 5.1.4. Substituting forward difference in time to equation (5.3) and assuming that cell volumes and areas are steady we obtain

$$\frac{\psi^{n+1}_{ijk} - \psi^n_{ijk}}{\Delta t} V - q^n_{ijk} V + \sum_{\partial\Omega_m} \Phi^n_m \partial\Omega_j = 0, \tag{5.9}$$

where summation is over the faces of cell i, j, k and Φ_m is the flux normal to face $\partial\Omega_m$. Similarly substituting backward difference in to equation (5.3) we obtain

$$\frac{\psi^{n+1}_{ijk} - \psi^n_{ijk}}{\Delta t} V - q^{n+1}_{ijk} V + \sum_{\partial\Omega_m} \Phi^{n+1}_m \partial\Omega_j = 0. \tag{5.10}$$

The difference between equations (5.9) and (5.10) is that fluxes and source terms are evaluated at different time. The first scheme (5.9) is also *explicit* as it does not involve equation solving at each step, because fluxes are known at time step n. The second scheme (5.10) is called *implicit* as opposed to explicit as fluxes are evaluated at the following time step $n+1$ and need to be solved.

Now combining the equations (5.9) and (5.10) we obtain

$$\frac{\psi_{ijk}^{n+1} - \psi_{ijk}^{n}}{\Delta t} + \frac{1}{2}\left(-\left(q_{ijk}^{n} + q_{ijk}^{n+1}\right) + \sum_{\partial\Omega_m}\left(\Phi_m^n + \Phi_m^{n+1}\right)\frac{\partial\Omega_m}{V}\right) = 0. \tag{5.11}$$

Equation (5.11) is known as the Crank-Nicolson scheme. If cell faces have equal area and the ratio of cell face area to cell volume is constant we may write

$$\frac{V}{\partial\Omega_m} = \Delta x, \tag{5.12}$$

where Δx is constant.

If the underlying problem is thought to be steady less accurate methods in time like (5.9) can be used instead of Crank-Nicolson scheme. However even in the steady case time derivatives are not usually omitted and problem is solved as a nonsteady problem, marching time onward until solution converges in time. This is due to a change of the problem type from parabolic to elliptic.

The main problem with the Crank-Nicolson scheme is that it may give rise to numerical oscillations in time referred to as *numerical dispersion*, which are undesirable. First order methods do not show this behavior, but give less accurate answers due to a lower order of convergence.

A discretization routine replaces the original PDE with a system of equations connecting the values of functions in different cells. If the underlying PDE is linear then this equation system is linear. However if the PDE is nonlinear then the equation set is nonlinear. Since RANS equations are nonlinear the obtained system of equations after FVM discretization is nonlinear [2, 13].

5.1.4 Error analysis

In this chapter we derive O-functions for each finite difference formula and discuss briefly the numerical stability of different schemes.

Recall that any function $\psi \in C^\infty(\mathbb{R})$ has a Taylor series expansion given by

$$\psi(x + \Delta x) = \sum_{n=0}^{\infty} \frac{\psi^n(x)}{n!} \Delta x^n, \tag{5.13}$$

where $\psi^n(t)$ is the n:th derivative at point t.

Using a Taylor series expansion for the forward difference formula we obtain

$$\frac{\psi(t + \Delta t) - \psi(t)}{\Delta t} = \frac{\sum_{n=1}^{\infty} \frac{\psi^n(t)}{n!} \Delta t^n}{\Delta t} = \frac{\partial \psi(t)}{\partial t} - O(\Delta t).$$

Thus the local error which is also called *truncation error* caused by this discretization is of order $O(\Delta t)$. For the central difference formula we obtain

$$\begin{aligned} \frac{\psi(t + \Delta t) - \psi(t - \Delta t)}{2\Delta t} &= \frac{\sum_{n=0}^{\infty} \frac{\psi^n(t)}{n!} \Delta t^n - \sum_{n=0}^{\infty} \frac{\psi^n(t)}{n!} (-\Delta t)^n}{2\Delta t} \\ &= \frac{\partial \psi(t)}{\partial t} + \frac{\sum_{n=3}^{\infty} (1 - (-1)^n) \frac{\psi^n(t)}{n!} \Delta^n}{\Delta t} = \frac{\partial \psi(t)}{\partial t} - O(\Delta t^2), \end{aligned}$$

which has second order accuracy due to $O(\Delta t^2)$. To obtain the truncation error of the Crank-Nicolson scheme we need to consider PDE

$$\frac{\partial \psi}{\partial t} = F, \tag{5.14}$$

where F is a function of x,t,ψ and spatial derivatives of ψ. Invoking Taylor expansion at time t to forward difference formula we obtain

$$\frac{\psi(t + \Delta t) - \psi(t)}{\Delta t} - F(t) = \frac{\sum_{n=1}^{\infty} \frac{\psi^n(t)}{n!} \Delta t^n}{\Delta t} - F(t). \tag{5.15}$$

Similarly invoking Taylor expansion at time $t + \Delta t$ to the backward difference formula we obtain

$$\frac{\psi(t + \Delta t) - \psi(t)}{\Delta t} - F(t + \Delta t) = \frac{\sum_{n=1}^{\infty} \frac{\psi^n(t + \Delta t)}{n!} (-\Delta t)^n}{\Delta t} - F(t + \Delta t). \tag{5.16}$$

Summing equation (5.15) and (5.16) we obtain

$$
\begin{aligned}
& 2\frac{\psi(t+\Delta t)-\psi(t)}{\Delta t} - (F(t+\Delta t)+F(t)) \\
= \;& \left(\psi^1(t+\Delta t)+\psi^1(t)\right) - (F(t+\Delta t)+F(t)) + \sum_{n=2}^{\infty}\left(\psi^n(t+\Delta t)-(-1)^n\psi^n(t)\right)\Delta^{n-1} \\
= \;& 0+0+\Delta t\left(\sum_{k=1}^{\infty}\psi^k(t)\Delta t^k\right) + \sum_{n=3}\left(\psi^n(t+\Delta t)-(-1)^n\psi^n(t)\right)\Delta t^{n-1} = O(\Delta t^2),
\end{aligned}
$$

thus the Crank-Nicolson scheme has a second order time accuracy. Next we consider accuracy in space. Let Φ be normal of flux to of certain face. Let Δx be distance from the middle of a cell to the face. Invoking Taylor series expansion to the flux we obtain

$$\Phi(x+\Delta x) = \sum_{n=0}^{\infty}\frac{\Phi^n(x)}{n!}\Delta x^n. \tag{5.17}$$

We may write a similar expansion for the adjacent cell obtaining

$$\Phi(x-\Delta x) = \sum_{n=0}^{\infty}\frac{\Phi^n(x)}{n!}(-\Delta x)^n. \tag{5.18}$$

As we evaluate fluxes by averages we get

$$
\begin{aligned}
\frac{\Phi(x+\Delta x)+\Phi(x-\Delta x)}{2} &= \frac{1}{2}\left(\sum_{n=0}^{\infty}\frac{\Phi^n(x)}{n!}\Delta x^n + \sum_{n=0}^{\infty}\frac{\Phi^n(x)}{n!}(-\Delta x)^n\right) \\
&= \Phi(x) + \frac{1}{2}\left(\sum_{n=2}^{\infty}\left(1+(-1)^n\right)\frac{\Phi^n(x)}{n!}\Delta x^n\right) \\
&= \Phi(x) + O(\Delta x^2).
\end{aligned}
$$

Hence the central-cell scheme yields a second order space accuracy.

Another important property of a method is stability. Discretization introduces some error to solution as discussed earlier. Another source of error is the *round-off error* caused by the floating point presentation of computers. Stability concerns involve growth of error over time. If these errors grow without limit over time a method is considered *unstable*. If a method does not show this kind of behavior it is considered *stable*. Stability depends on the problem, the solution method and properties of the mesh.

Recall discretized equation (5.11) and multiply both sides by Δt we obtain

$$\psi_{ijk}^{n+1} - \psi_{ijk}^{n} + \frac{1}{2}\left(- \left(q_{ijk}^{n} + q_{ijk}^{n+1} \right) \Delta t + \sum_{\partial\Omega_m} \left(\Phi_m^n + \Phi_m^{n+1} \right) \frac{\Delta t}{\Delta x} \right) = 0. \tag{5.19}$$

The ratio of the time step and the space step (cell length) multiplied by velocity is called the Courant number. The Courant number is given by

$$C_\nu = \frac{u \Delta t}{\Delta x}. \tag{5.20}$$

A sufficient condition for stable simulation in case of RANS equations is that $C_\nu \leq 1$ [2]. Physically Courant number presents the ratio of space discretization to the distance that fluid particle can travel in single time step. Thus it demands that fluid should not be able to cross multiple cells in one time step. Similarly if the Courant number is very small it takes multiple time steps to cross a single cell and space accuracy is unnecessarily fine. For this reason Courant number for hyberbolic PDEs should be close to one, which secures optimal performance.

It should be noted that some methods like Crank-Nicholson are unconditionally stable and do not require the Courant number to be less than 1. Implicit schemes such as backward difference are also more stable than explicit schemes such as forward difference and give more freedom in choosing the time step [2, 13, 15, 1].

5.2 Equation linearization

As discretization of RANS equations leads to nonlinear equations it is customary to use some linearization procedure to transform them into linear equations. There are currently many different ways to achieve this and how linearization should be done depends on the nature of the problem, mainly whether the problem is considered to be steady or unsteady and if the problem is compressible or incompressible. In this section we will look at linearization techniques designed for compressible flows.

Most commonly used methods (SIMPLE, SIMPER, SIMPLEC, PISO,...) consist of Predictor-Corrector schemes employed between timesteps. We will present the SIMPLE and PISO algorithms for compressible flows.

Conservation of mass and momentum coupled with a state equation for instance the ideal gas law, enables solution for pressure, density and the velocity field if a temperature distribution is given. Similarly if pressure, density and velocity are given we may solve the temperature distribution from the energy conservation equation. This splitting of equations is known as a *segregated* solution. If temperature is solved

simultaneously with velocity and other values than solution is called *coupled*. In the segregated case each iteration begins with solution of velocity, pressure and density from the previous time steps temperature distribution. After this the temperature is solved from the energy equation using the current velocity, pressure and density.

Superscript notation for time and subscript for cell will be used. For instance u_i^n is velocity component in cell i at time n.

The discretized conservation of momentum equation in a implicit case is given by

$$A_C u_C^{n+1} + \sum_k A_k^u u_k^{n+1} = Q_u^{n+1} - \left(\frac{\Delta p^{n+1}}{\Delta x}\right)_C, \tag{5.21}$$

where u is some velocity component, C is the index of cell for which equation is writen, x is a coordinate in the same direction as u and $\Delta/\Delta x$ refers to the spatial discretization scheme of derivative. Summation $\sum_k$ is done over neighboring cells. Coefficient matrices A_k^u may depend on u and thus equation (5.21) is nonlinear. Moreover source matrix Q_u^{n+1} may depend on u in a nonlinear way. However if we treat coefficient matrices A_k^u as constants equation (5.21) is linearized.

In the case of backward difference conservation of mass is given by

$$\frac{\rho_C^m - \rho_C^n}{\Delta t} + \frac{\Delta \rho^m u^m}{\Delta x} = 0. \tag{5.22}$$

Solution of linearized equations typically consists of two kinds of iterations, namely outer and inner iterations. In *outer iterations* the coefficient matrices A_k and the source matrix Q_u^{n+1} are updated. In *inner iterations* linear equation obtained from equation (5.21) is solved.

Let u_i^{m*} be the solution of the present (outer) iteration. The present solution has to satisfy equation (5.21) with a given tolerances. Solving u_C^{m*} from equation (5.21) we obtain

$$u_C^{m*} = -A_C^{-1}\left(\sum_k A_k^u u_k^{m*} + \left(\frac{\Delta p^{m-1}}{\Delta x}\right)_C - Q_u^{m-1}\right), \tag{5.23}$$

where $m-1$ refers to the previous outer iteration. Velocity u^{m*} can be thought as a predicted velocity in a Predictor-Corrector scheme.

However u^{m*} does not generally satisfy the conservation of mass equation. Our aim is to introduce corrections to involved variables u, ρ and p such that after the correction(s) they do satisfy both the conservation of mass and conservation of momentum

equation (5.21). We will denote correction with a comma $'$. For instance $u^m = u^{m*} + u^{'}$, where $u^{'}$ is the correction.

5.2.1 SIMPLE

SIMPLE (Semi-Implicit Method for Pressure-Linked Equations) method is one way to correct velocity, pressure and density to satisfy conservation of mass equation. The SIMPLE method is usually used only in steady calculations, where time accuracy is not crucial.

The main idea of SIMPLE is that a correct velocity can be obtained by correcting pressure alone. Thus SIMPLE is omitting the effect of neighboring cell velocities and their corrections. This allows us to write

$$u_C^m = -A_C^{-1}\left(\sum_k A_k^u u_k^{m*} + \left(\frac{\Delta p^m}{\Delta x}\right)_C - Q_u^{m-1}\right). \tag{5.24}$$

Substracting equation (5.23) from equation (5.24) yields

$$u_C^{'} = -A_C^{-1}\left(\frac{\Delta p^{'}}{\Delta x}\right)_C. \tag{5.25}$$

Moreover pressure correction $p^{'}$ is connected to density correction $\rho^{'}$ by equation of the state. Hence

$$\rho^{'} = \left(\frac{\partial \rho}{\partial p}\right)_T p^{'} = C_\rho p^{'}, \tag{5.26}$$

where C_ρ is a coefficient depending on the temperature T. Before any correction present solution of momentum equations u_i^{m*} satisfies

$$\frac{\rho_C^{m-1} - \rho_C^n}{\Delta t} + \frac{\Delta \rho^{m-1} u^{m*}}{\Delta x} = \Delta \dot{m}, \tag{5.27}$$

where $\Delta \dot{m}$ presents imbalance in the conservation of mass equation. Invoking the definition of correction and subtracting equation (5.27) from equation (5.22) we obtain

$$\frac{\rho^{'}}{\Delta t} + \left(\frac{\rho^{m-1} u^{'} + \rho^{'} u^{m*} + \rho^{'} u^{'}}{\Delta x}\right)_C + \Delta \dot{m} = 0. \tag{5.28}$$

Corrections are usually small, hence it is customary to omit the product term $\rho' u'$. Substituting density correction (5.26) and velocity correction (5.25) to equation (5.28) we obtain the pressure correction formula of the compressible SIMPLE method

$$\frac{C_\rho p'_C}{\Delta t} + \left(\frac{\Delta(C_\rho u^{m*} p')}{\Delta x}\right)_C + \frac{\Delta}{\Delta x}\left(A_C^{-1}\rho^{m-1}\left(\frac{\Delta p'}{\Delta x}\right)\right)_C = -\Delta\dot{m}. \tag{5.29}$$

Equation (5.29) can be used to the solve pressure correction at each outer iteration. Moreover pressure correction can be used to correct velocity and density and other properties.

Due to omission of neighboring velocities, pressure corrections calculated via the SIMPLE method are too large. This defect can be corrected by employing an under-relaxation scheme. The main idea of under-relaxation is to only use a fraction of the correction. This can be expressed as

$$p^m = p^{m-1} + \alpha_p p', \tag{5.30}$$

where $\alpha_p \in [0, 1]$.

Moreover velocity has to be under-relaxed. This is usually done implicitly by modifying the momentum equation (5.21) to

$$\frac{A_C}{\alpha_u} u_C^{m*} + \sum_k A_k^u u_k^{n+1} = Q_u^{n+1} - \left(\frac{\Delta p^{n+1}}{\Delta x}\right)_C + (1-\alpha_u)\frac{A_C}{\alpha_u} u_C^{m-1}. \tag{5.31}$$

Under-relaxation factors should be chosen such a way that they allow as fast a convergence as possible. For given α_u optimal α_p is given by

$$\alpha_p = 1 - \alpha_u. \tag{5.32}$$

Interestingly for given α_u it is possible to change values of α_p over some range of values without affecting the convergence of the method [15, 1].

5.2.2 PISO

The PISO (Pressure Implicit with Splitting of Operators) method is another way of calculating pressure corrections. The main difference between the PISO method and the SIMPLE method is that the PISO method employs multiple correction stages.

Moreover as SIMPLE is used mainly in steady calculations, the PISO method is usually used in unsteady calculations.

The first step of the PISO method is same as in the SIMPLE method. Pressure correction is calculated by equation (5.29). However after this the PISO method employ a number of additional correction stages.

Additional correction stages take account the effect of neighboring cells by

$$u^{(m-1)} + u^{(m)} = -A_C^{-1}\left(\sum_k A_k u_k^{(m-1)} + \left(\frac{\Delta p^{(m-1)}}{\Delta x} + \frac{\Delta p^{(m)}}{\Delta x}\right)_C\right), \tag{5.33}$$

where (m) and $(m-1)$ refer to correction stages, i.e. $u^{(1)} = u^{'}$ and $p^{(2)}$ is the second correction term of pressure.

Invoking equation (5.25) to equation (5.33) and solving for present correction we obtain

$$u_C^{(m)} = -A_C^{-1}\left(\sum_k A_k u_k^{(m-1)} + \left(\frac{\Delta p^{(m)}}{\Delta x}\right)_C\right). \tag{5.34}$$

Assuming that after correction (m), velocity and density satisfy conservation of mass equation and omitting the mixed correction term $\rho^{(m)}u^{(m)}$ we obtain

$$\begin{aligned}\frac{C_\rho p_C^{(m)}}{\Delta t} + \frac{\Delta(u_C^{m-1} C_\rho p_C^{(m)}}{\Delta x} &- \frac{\Delta}{\Delta x}\left(A_C^{-1}\rho_C^{m-1}\sum_k A_k u_k^{(m-1)}\right) \\ &- \frac{\Delta}{\Delta x}\left(A_C^{-1}\rho_C^{m-1}\frac{\Delta p_C^{(m)}}{\Delta x}\right) = 0.\end{aligned} \tag{5.35}$$

In the original paper of Issa [11] only one additional correction step (5.35) is employed. However in present CFD software the correction step (5.35) is used in an iterative fashion until correction terms converge to zero under some tolerances. Moreover the PISO method does not need under-relaxation like the SIMPLE method. This is because the PISO method is taking into account velocity corrections of neighboring cells which are omitted in SIMPLE [15, 1].

5.3 The algorithm

In this section we discuss briefly how the actual algorithm proceeds. We restrict our discussion to the segregated case. Segregated solvers are more widely used than coupled solvers as they are computationally less expensive. The main advantage of coupled solver lies in supersonic flows, where temperature is strongly coupled to flow velocity.

In the very beginning of the simulation the domain is partitioned into a mesh, solution fields (pressure, velocity, etc.) are initialized and boundary conditions are set. With initializion we mean initial values before any time steps. In the steady case velocity and pressure values can be set to zero or to some ambient value. However this may create discontinueties in gradients, which may become problem if they grow too large.

After initialization time is marched onward and values at each time step are determined from previous values. Each time step consists of outer and inner iterations. As discussed in section 5.2 first equations are linearized. Events taking place in the outer iterations are described in the following list [15]:

1. Solve the linearized momentum equation and obtain updated velocity (inner iterations).
2. Correct velocity, pressure and density using the pressure correction method (SIMPLE, PISO, etc.).
3. Solve the temperature from the linearized energy equation.
4. Solve the $k - \varepsilon$ turbulence model and update turbulence viscosity.
5. Update coefficients of linearized equations by using the latest properties.
6. Return to step 1 until all corrections become small (under some tolerance).
7. Advance to the next time step.

Most of the computation time is spend in solving linear equations. Linear equations arising from PDEs are typically very large, but sparse. Thus special methods are needed to solve these equations efficiently. Sparse linear equation solvers are typically iterative in contrast to gaussian elimination, which is a direct algorithm. Most widely used algorithms are the algebraic multigrid method (AMG) and the conjugate gradient method [15, 1].

Chapter 6

Simulation of nozzle flow

6.1 Boundary conditions

In the nozzle simulation, there are three different types of boundaries: solid boundaries, pressure inlet and outlets and symmetry. Solid boundaries are surfaces that do not permit any fluid flow through themselves. However, in fluid dynamics, it is customary to also require that velocity vanishes at these boundaries, in contrast to electromagnetism where it is usually required that only the normal component of the electric field vanishes at the surface of the conducting material. This difference can be explained by the presence of viscous forces which slow fluid flow near the solid boundaries. Sometimes the heat flux through a solid boundary is modelled by specifying a temperature distribution on the wall, but in this thesis we assume that the heat flux through these boundaries is negligible and omit it. This assumption can be justified by the very short operation time of lasers, which leads to a very small heat flux through the nozzle walls. Moreover it is essential that the nozzle walls are modelled in simulation exactly as they are modelled in the CAD model. This means that the mesh must be cut in the same shape to satisfy the CAD model. This requirement is due to sensitivity of the flow to variations of the nozzle throat.

Symmetry planes are boundaries where fluid flow is assumed to continue as the same after the boundary. The main advantage in using this kind of boundaries is in making the computational domain smaller. This saves computation time and increases the reliability of the solution. A symmetry boundary can be modeled by taking the normal velocity and normal gradients of all variables to be zero.

A pressure inlet is a kind of free flow boundary, where sufficient fluid properties are given. These properties usually include pressure, temperature and velocity, but other combinations are also possible. These combinations may consist of for instance, some

combination of stagnation properties or a requirement for the overall mass flux through the inlet. A pressure outlet is also a free flow boundary in which the gradients of all variables along the flow direction are taken to be zero and the exit mass flow is fixed to satisfy overall conservation of mass [1].

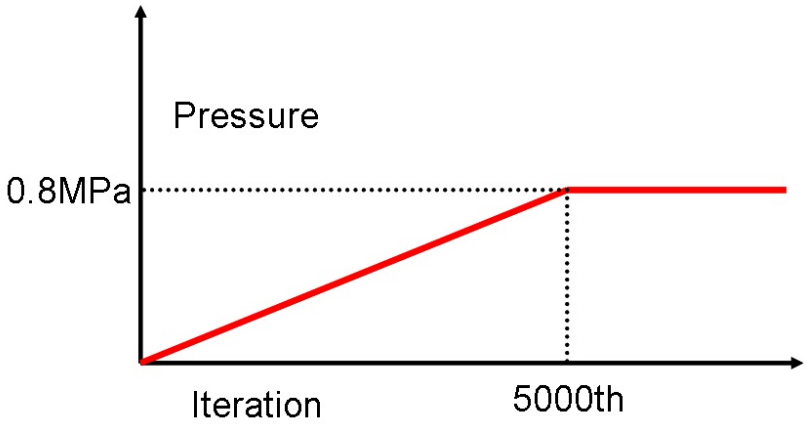

Figure 6.1: Figure illustrating the increase of pressure during the simulation.

Pressure was increased slightly at each iteration at the inlet in order to avoid large pressure gradients. Pressure was set as 0Pa at beginning and increased to 0.8MPa by the 5000th iteration by increasing pressure by 160Pa at each iteration. This is illustrated in Figure 6.1.

6.2 Meshing routines

We use two different types of meshes: a prism layer mesh near the solid boundaries and a polyhedral mesh elsewhere. A prism layer mesh consists of thin slices near the wall that stretch when moved farther from the boundary. It is common to use a wall model in this type of a mesh. There are typically one to five layers of prism layer mesh in solid boundaries.

A polyhedral mesh consists of volume divided into polyhedrons. As FVM allows considerable freedom in meshing it is customary to make the mesh finer (smaller cells) in some domains. In this thesis finer mesh was used at the nozzle and at the symmetry plane. Because the symmetry plane was also the observed plane and the throat is crucial region for whole flow. Meshing parameters of this thesis can be found from appendix A.

6.3 Methods

The simulation results were obtained by a segregated solver. Computation was executed in nonsteady fashion with a 1st order in time discretization method. Space discretization was 2nd order.

Moreover the under-relaxation factors were changed over time in a ramp fashion similar to pressure. This is because using a large under-relaxation factor at the early iterations seemed to have the effect of crashing the simulation. However if the under-relaxation factors were kept small, the simulation usually resulted in a crash at the later stages of simulation. In this context the crash should be understood as a floating point exception which halted the simulation.

We used two viscosity models, namely the Sutherland law and a constant viscosity model. This was due to difficulties associated with the Sutherland law. The gas was modelled as an ideal gas.

Parameters associated with the computation algorithms can be found at appendix A.

6.4 Simulation results

The simulated nozzles diameter was 1.0 mm. Used parameters can be found at appendix A.

Figure 6.2 shows the velocity distribution of the laval nozzle. We computed the velocity profile both using the Sutherland law and without the Sutherland law.

Figure 6.3 shows the density distribution of the laval nozzle. We computed velocity profile both using the Sutherland law and without the Sutherland law.

Figure 6.4 and Figure 6.5 shows the residuals of both computations. Iterations in the figures include outer and inner iterations.

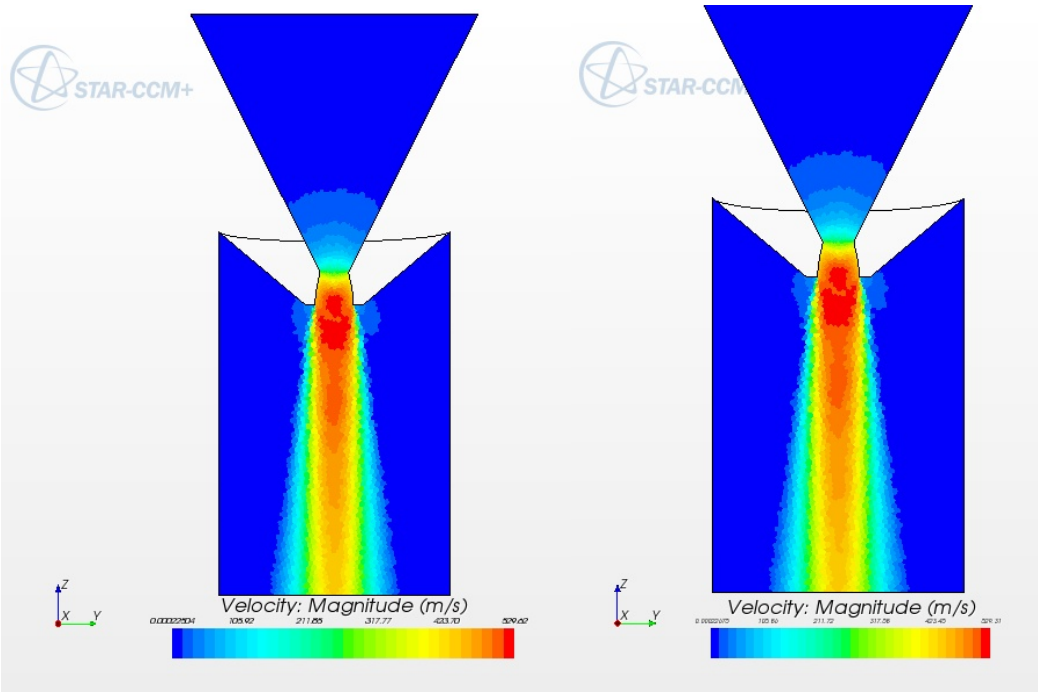

(a) Laval nozzle with the Sutherland law.

(b) Laval nozzle without the Sutherland law.

Figure 6.2: Pictures of the velocity profiles of the laval nozzle. In first picture (A) solution is obtained using the Sutherland law and in second picture (B) without the Sutherland law.

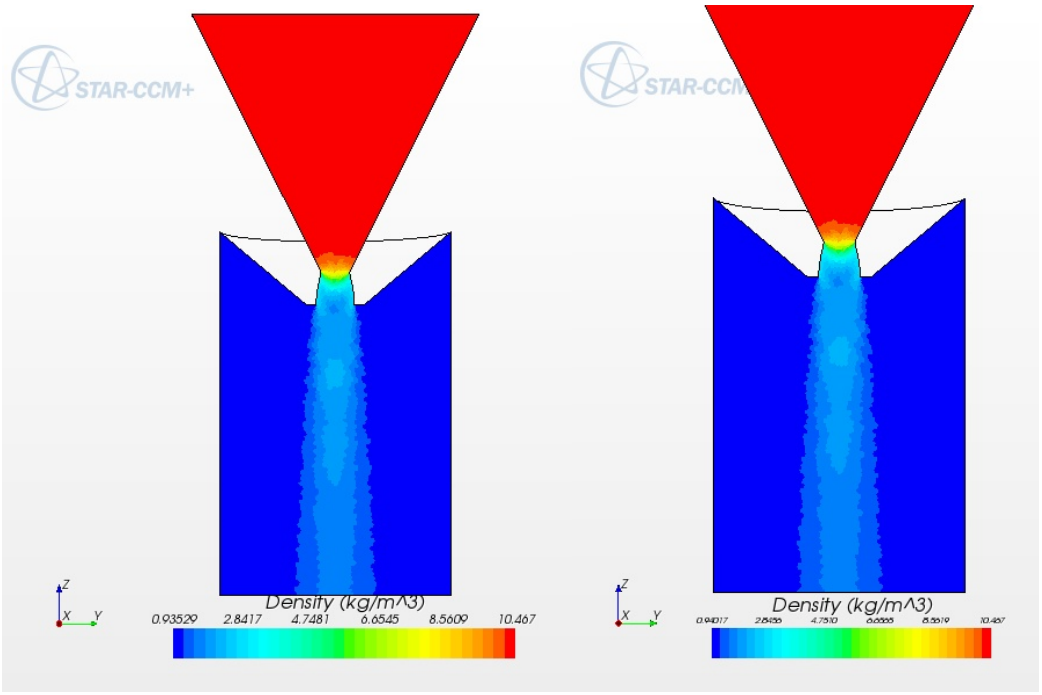

(a) Laval nozzle with the Sutherland law.

(b) Laval nozzle without the Sutherland law.

Figure 6.3: Pictures of density profiles of the laval nozzle. In first picture (A) solution is obtained using the Sutherland law and in second picture (B) without the Sutherland law.

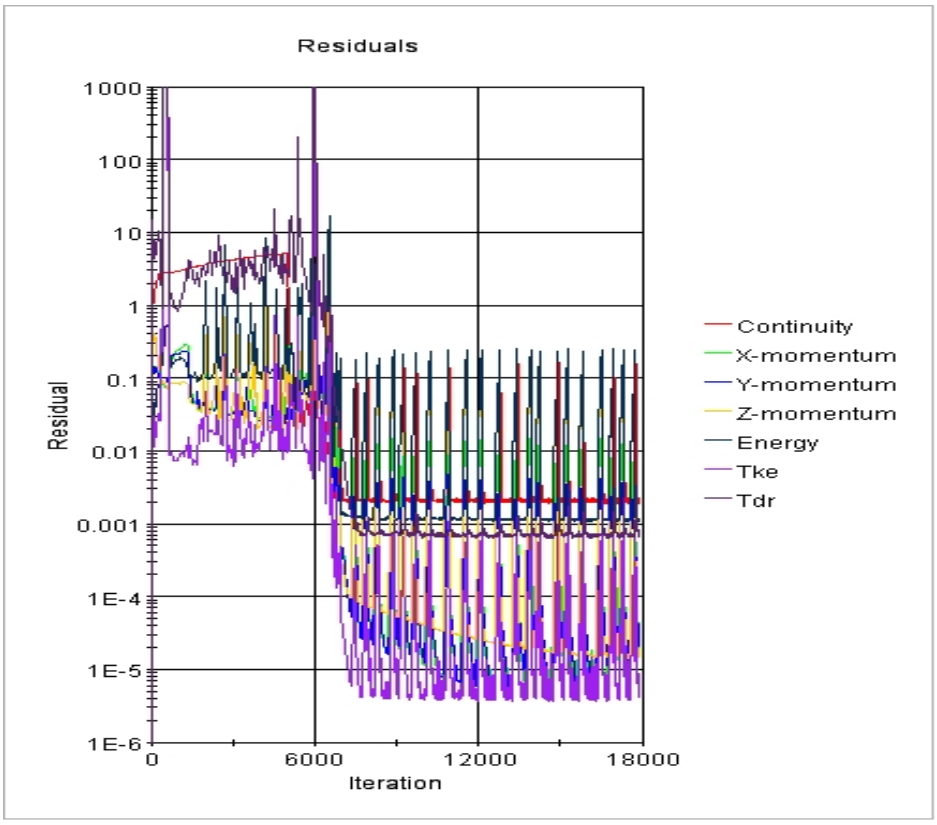

Figure 6.4: A picture showing residual convergence when the Sutherland law was used.

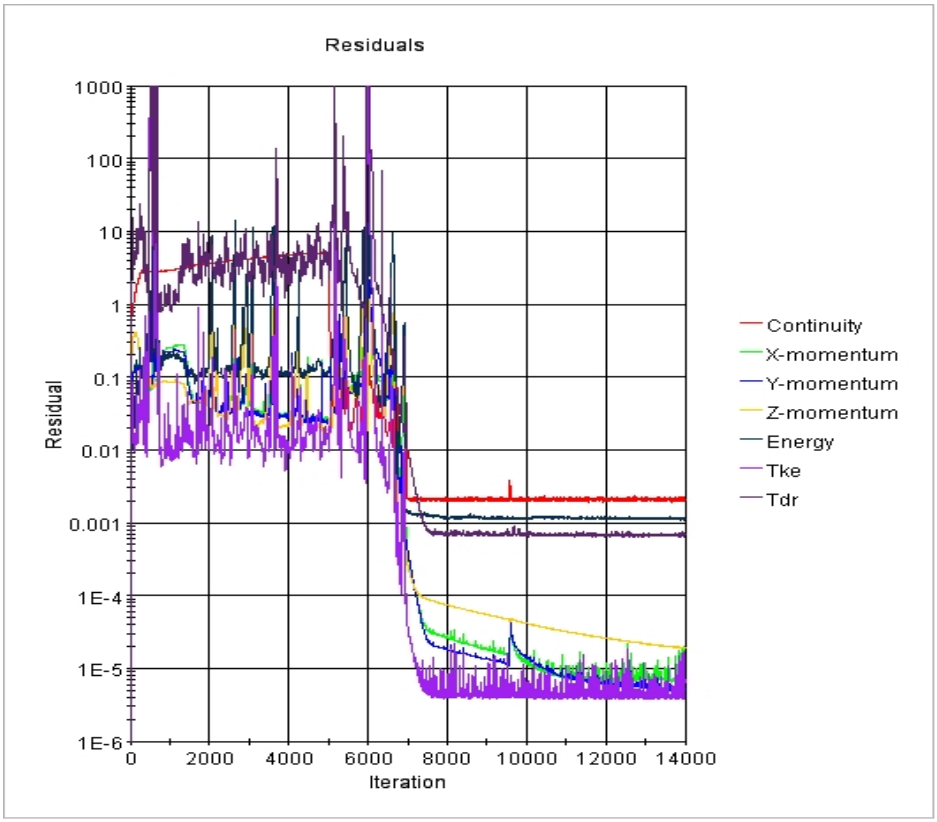

Figure 6.5: A picture showing residual convergence when the Sutherland law was not used.

Chapter 7

Measurements

7.1 Theory of Schlieren photography

Schlieren photography is an experimental setup to observe density gradients. It is based on the fact that the refractive index of a gas depends on its density. Thus density gradients can be observed from the refraction difference of collimated light. The light is focused using a lens and a knife edge is placed at the focal point of the focused beam. Figure 7.1 shows a schematic picture of a Schlieren system.

Succesfull knife edge blocks around half of the focused light. In an uniform flow this will only cause the brightness of image to decrease. However if there are density gradients present in the flow, the knife edge will cause beams to focus imperfectly and block parts of light focused in the knife edge. The result is that there are darker areas at positive and negative density gradients in the direction normal to the knife-edge [21].

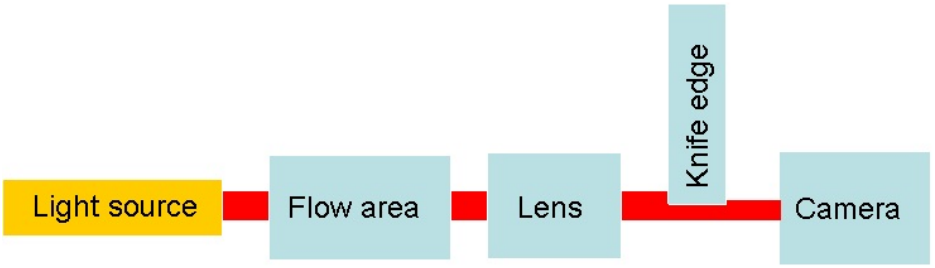

Figure 7.1: Schematic picture of a Schlieren system.

7.2 The Schlieren photographs

In this thesis a He-Ne laser was used as a illumination source. Figures 7.2 and 7.3 show Schlieren images of the nozzle at 0.80MPa. The nozzle was rotated between each photograph, which explains the different positions of the shock waves. The nozzle diameter was 1.0 mm.

In a perfect nozzle all of the photographs should have the same shape of jet. However due to an imperfect machining and a turbulent eddies already present in the inlet of the nozzle, the nozzle shape is distorted.

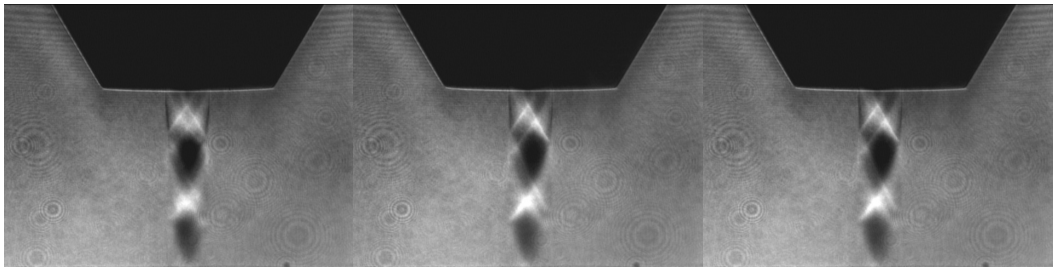

(a) (b) (c)

Figure 7.2: Schlieren photographs of the nozzle.

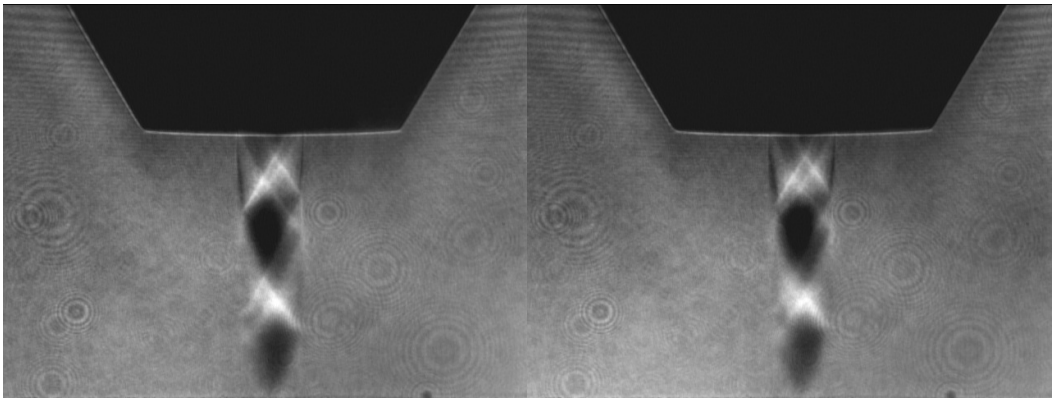

(a) (b)

Figure 7.3: Schlieren photographs of the nozzle.

Chapter 8

Conclusions

In this thesis the theoretical basis of modeling high speed assist gas flow was presented. The Star-CCM+ CFD software was evaluated for simulating such a model. We omitted the effect of removed metal particles and chemical reactions of the assist gas in the kerf. The simulation results were compared to a measurements. The measurements were done by a Schlieren photography and pressure on workpiece. The Schlieren photography can be mainly used to observe the jet shape and the shockwave positions, but lack any accurate information about the actual velocities. Pressure on workpiece can be used to determine if the simulated pressure is close to the actual pressure. The measurements can be found from section 7.2.

Comparing simulation results to the Schlieren photographs and pressure on workpiece, it can be concluded that software achieved sufficient accuracy.

Moreover it was concluded that using a simple segregated solver instead of a computationally more expensive coupled solver was sufficient to achieve correct shape of jet, which can be observed from the Schlieren photographs. This feature is especially desirable when the model is made more complex by addition of molten metal particles or by presence of chemical reactions of oxygen with metal in the kerf.

We also simulated dynamic viscosity with the Sutherland law and with a constant value model. The Sutherland law introduced oscillations in the residuals. Moreover the two solutions were very close to each other, which suggests that use of the Sutherland law may be unnecessary.

References

[1] Star-d version 3.15 methodology, 2001.

[2] Dale A. Anderson, John C. Tannehill, and Richard H. Pletcher. *Computational Fluid Mechanics and Heat transfer.* Hemisphere Publishing Corporation, New York, 1984.

[3] G. M. Anderson. *Thermodynamics of Natural Systems.* Wiley, Toronto, 1996.

[4] Todd Arbogast and Jerry L. Bona. *Methods of Applied Mathematics.* University of Texas Austin, Texas, 2007.

[5] Dennis S. Bernstein. *Matrix Mathematics.* Princeton University Press, Princeton, 2005.

[6] John Dowden. *The Theory of Laser Materials Processing.* Springer, Essex, 2008.

[7] D. S. Drumheller. *Introduction to Wave Propagation in Nonlinear Fluids and Solids.* Campridge University Press, Campridge, 1998.

[8] Sirkka-Liisa Eriksson. Lecture notes of funktionaalianalyysin jatkokurssi, 2010. Tampere University of Technology.

[9] P. R. Garabedian. *Partial Differential Equations.* Wiley, New York, 2nd edition, 1964.

[10] D. Gilbard and N. S. Trudinger. *Elliptic Partial Differential Equations of Second Order.* Springer, Berlin, 2nd edition, 1983.

[11] R. I. Issa. Solution of the implicitly discretised fluid flow equations by operator-split. *Journal of Computational Physics*, 1984.

[12] Reijo Karvinen. Lecture notes of virtausoppi, 2010. Tampere University of Technology.

[13] O. Kolditz. *Computational Methods in Enviromental Fluid Mechanics.* Springer, London, 2002.

[14] Dilip Kondepudi and Ilya Prigogine. *Modern Thermodynamics*. Wiley, West Sussex, 1999.

[15] Andreas Meister and Jens Struckmeier. *Hyperbolic Partial Differential Equations*. Vieweg, Hamburg, 2002.

[16] Yasuhiro Okamoto, Yoshiyuki Uno, and Hiroshi Suzuki. Effect of nozzle shape on micro-cutting performance of thin metal sheet by pulsed nd: Yag laser. *International Journal of Automation Technology*, 4(6), 2010.

[17] David V. Ragone. *Thermodynamics of Materials Volume I*. Wiley, Massachusetts, 1995.

[18] Walter Rudin. *Real and Complex Analysis*. McGraw-Hill Book Company, Wisconsin, 3rd edition, 1966.

[19] Walter Rudin. *Functional Analysis*. Tata McGraw-Hill LTD, New Delhi, t m h edition edition, 1974.

[20] William M. Steen. *Laser Material Processing*. Springer, London, 3rd edition, 1998.

[21] Ikui Takehumi and Matsuo Kazuyasu. *Assha Kuseiryuutai Norikigaku*. Rikungaku-sha, Tokyo, 19th edition, 1977.

[22] Hiroki Tanabe. *Functional Analytic Methods for Partial Differential Equations*. Marcel Dekker Inc, New York, 1997.

Appendix A

Simulation parameters

This chapter explains the parameter values. Each parameter is accompanied by a short explanatory note. Table A.1 describes parameters associated with mesh generation.

Parameter name	Description	Value
Base size	Reference value to all mesh lengths	0.3mm
Numb. Prism layer meshes	Layer number in the prism layer mesh	2
Prism layer stretching	Ratio of consecutive layers thicknesses	1.5
Prism layer thickness	Percentage of base size	20%
Surface curvature	Percentage of base size	36%
Surface growth rate	Number of cell layers grown next to boundary	1.3
Rel. min. size	Percentage of base size	25%
Rel. target size	Percentage of base size	100%
Wrap. feat. angle	Max. angle of surface features	15°
Wrap. scale factor	Scaling of surface	15%

Table A.1

Moreover in the nozzle throat and the nozzle outlet custom values were used. These custom values are given in the following Table A.2.

Parameter name	Description	Value
Base size	Percentage of default base size	10%
Rel. min. size	Percentage of base size	10%
Rel. target size	Percentage of base size	20%

Table A.2

Table A.3 describes parameters associated with numerical solvers.

Parameter name	Description	Value
Inner iteration	Max. Numb. of inner iterations	100
Time step	Time step between outer iterations	0.004s
Velocity un.-rel. factor	Final value of under-relaxation factor	0.15
Pressure un.-rel. factor	Final value of under-relaxation factor	0.7
Energy un.-rel factor (fluid)	Enthalpy for fluid	0.5
Energy un.-rel factor (solid)	Enthalpy for solids	0.99
k-ε turb. un.-rel factor	Turbulence model under relaxation	0.8
k-ε turb. visc. un,-rel factor	Turbulent viscosities under relaxation	0.99

Table A.3

The ramps used in this thesis are described in the Table A.4.

Property name	End iteration	Initial value	Final value
Pressure	5000	0	800kPa
Velocity under-rel. factor	1000	0.01	0.15
Pressure under-rel factor	1000	0.01	0.7

Table A.4